A Review and Functional Analysis of Space Charge Measurement Deconvolution Techniques for HVDC Cables

Alessio Di Fatta, *IEEE, Student Member*, Giuseppe Rizzo, Pietro Romano, *IEEE, Senior Member*, Guido Ala, *IEEE, Senior Member*, Antonino Imburgia, *IEEE, Member*

Abstract

As High Voltage Direct Current (HVDC) technology becomes increasingly important for the integration of large-scale renewable energy sources and to ensure efficient long-distance power transmission, an accurate assessment of insulation performance is necessary to maintain system reliability and minimize fault risks. In this scenario, the measurement of space charge in dielectric materials is useful for optimizing insulation systems for HVDC equipments. The Pulsed Electro-Acoustic (PEA) method is one of the most widely used techniques for space charge analysis, but distortions introduced by the measurement system significantly affect the accuracy of the acquired signals. Among the various factors influencing the acquisition of the space charge profile is the convolution process between the signal and the measuring cell, which is characterized by its own transfer function. Therefore, signal deconvolution is essential for accurately reconstructing the space charge distribution. This paper presents a comparative review of the deconvolution techniques suggested by researchers in the field of PEA measurement. Theoretical principles, advantages, and limitations of methods such as Fourier and Wiener deconvolution are analyzed, along with advanced solutions based on Laplace and Short Time Fourier Transforms. Furthermore, the techniques have been implemented and tested in a MATLAB environment for practical comparison. The results demonstrate how the choice of technique influences the quality of the reconstructed signal, providing optimal selection criteria for different experimental conditions.

Index Terms

Alessio Di Fatta, Pietro Romano, Guido Ala and Antonino Imburgia are with the L.E.PR.E. H.V. Laboratory, Department of Engineering, University of Palermo, Italy.

Giuseppe Rizzo is with Prysmian S.p.A., Milan, Italy.

HVDC Cable, Space Charge, PEA, Deconvolution Technique, Signal Processing.

I. Introduction

The transition to a sustainable energy future depends on efficient and reliable transmission systems capable of integrating large-scale renewable energy sources. High Voltage Direct Current (HVDC) technology has emerged as a key factor of this transition, ensuring long-distance power transmission with minimal losses [1]–[3]. However, the reliability of HVDC systems are strongly influenced by the performance of their insulation materials. For this reason, several researches have focused on the study of techniques to analyze and monitor their state of health [4], [5]. Measurement of space charge is becoming increasingly important in the evaluation of dielectric properties and in the understanding of degradation and failure phenomena [6]–[8]. The ability to evaluate the electric field profile, based on the acquired charge distribution, allows optimization of the insulation system design and management of a HVDC equipment, ensuring safe and reliable operation. Among the most widely used methods for obtaining information on space charge distribution, the Pulsed Electro-Acoustic (PEA) method stands out for its ability to provide high spatial resolution for measurements on reduced-scale and real cables [9]–[12]. However, the interpretation of PEA acquisitions can be influenced by distortions introduced by other mechanical and electrical components of the PEA measurement setup itself, as well as by environment noise [13]. In addition to the attenuation and dispersion effects caused by the dissipative nature of the dielectric medium and the cable geometry, distortions introduced by the transducer and amplifier used for signal detection further challenge the analysis. For these reasons, the measurement process requires a signal processing phase that aims to reconstruct the charge profile with good accuracy [14]–[16]. To address these issues, deconvolution techniques have taken on a pivotal role, enabling a more accurate reconstruction of the sensor input profile and improving the quality of experimental results. However, selecting the most appropriate deconvolution method remains a challenge due to the trade-offs between computational efficiency, noise suppression, and signal fidelity. This paper aims to provide a comprehensive review of the deconvolution techniques, for PEA measurement, available in literature, analyzing their theoretical principles, advantages, limitations, and practical applications. Furthermore, this work goes beyond a simple description of the techniques. Through implementation in MATLAB environment, a direct comparison of these methods is provided, allowing for an empirical evaluation of their performance in processing PEA signals. The ultimate goal is to establish

guidelines for selecting the most suitable deconvolution technique based on specific application and measurement conditions, optimizing the accuracy of space charge distribution analysis in HVDC cable insulation systems.

II. Convolution issue in PEA Measurement

The fundamental principle of the PEA method involves applying a voltage pulse to the device under test, generating an electroacoustic response detected by a transducer system. Specifically, when subjected to the voltage pulse, space charges within the dielectric experience a perturbation, inducing the generation of acoustic waves. These waves propagate through the material and reach the measurement cell, where they are detected. The PEA cell, which consists of an acoustic wave transmission system and a piezoelectric sensor, converts the pressure wave into an electrical signal proportional to the charge distribution. However, the measured signal does not directly correspond to the original space charge distribution due to convolution effects introduced by the system's response, as described by the following time domain expression [17]:

$$y(t) = h(t) * x(t) + n(t) \tag{1}$$

where $x(t)$ and $y(t)$ are the input signal received by the PEA cell (non-convolved profile) and the output signal (convolved profile), respectively. The system response, denoted $h(t)$, characterizes the response of the measurement cell, while $n(t)$ accounts for external noise contributions. It is important to note that $x(t)$ itself does not correspond to the original charge distribution within the dielectric, but serves as an intermediate signal that still requires further processing [16]. The attenuation and dispersion phenomena suffered by the profile and due to the dissipative nature of the dielectric medium and the geometry of the cable must also be corrected. These corrections are made by subsequent processing not included in this work for the sake of brevity. For an accurate interpretation of the measurement, it is necessary to retrieve the signal $x(t)$ with a process that is known as deconvolution. The next section will explore the deconvolution methods, emphasizing the theoretical principles and practical implications of each approach. The described techniques have been implemented using the MATLAB environment and applied to two space charge profiles obtained from separate measurements that have been performed on two HVDC cables with different scales and applied voltages. The first measurement has been conducted on a reduced scale, or model, cable at an applied voltage of 80 kV, while the second has been carried out on a full-size cable at 525 kV. Both tests have been performed using the

same PEA measurement cell, which has been originally designed and optimized for full-size HVDC cables [16], [18], [19]. As shown in Fig. 1 and Fig. 2, the space charge profile acquired for the model cable exhibits lower spatial resolution compared to the full-size cable. This is due to the mismatch between the dimensions of the model cable and the measurement system. As a result, finer details in the charge distribution are less distinguishable in the model cable measurement, while the full-size cable profile appears more defined and accurate. It should be noted that deconvolution techniques can only extract information present in the raw signal. Thus, while the algorithms remain valid and stable, the limited resolution of the acquired data restricts the level of detail that can be meaningfully reconstructed. However, the choice to report this comparison stems from an interest in investigating the differences that may emerge between these two application contexts. Model cables provide an ideal, controlled environment for validating algorithms, whereas full-size cables introduce the complexities inherent in practical, real-world scenario.

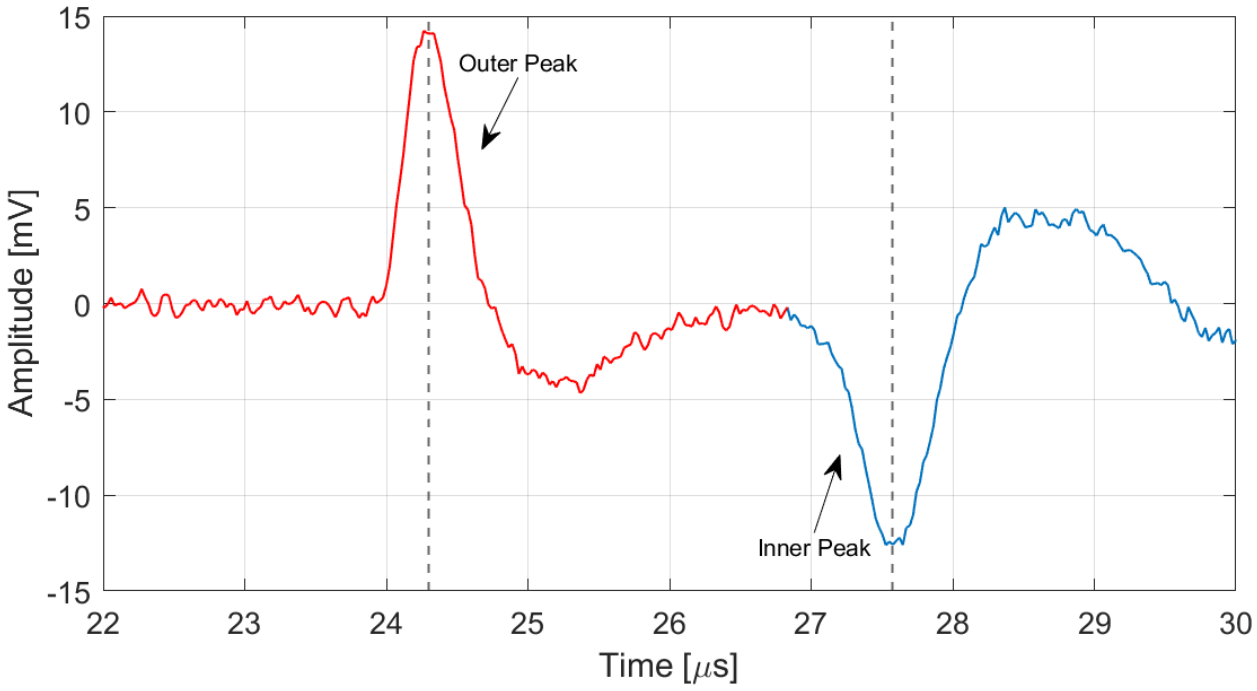

Fig. 1. Space charge profile acquired for model cable measurement. Applied voltage: 80kV.

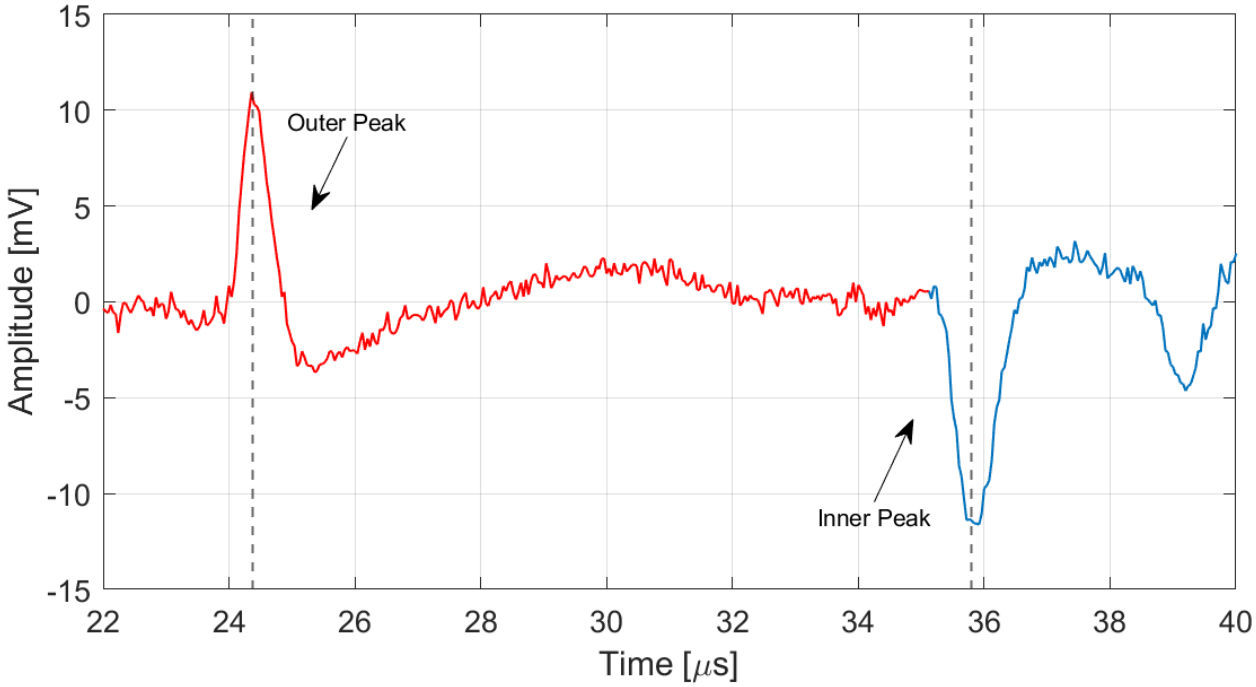

Fig. 2. Space charge profile acquired for full-size cable measurement. Applied voltage: 525kV.

III. Deconvolution Techniques

According to the previous section, deconvolution techniques are essential tools for enhancing data analysis, allowing the reconstruction of signals distorted by the characteristics of the measurement system. In this context, the techniques can be classified according to the way they act on the signal. Processing can be performed in the time domain, the frequency domain, or a hybrid combination of both. Another distinction factor among these techniques lies in their implementation approach. Some methods are based on iterative algorithms that progressively refine the solution through successive approximations, allowing for the correction of distortions step by step. These iterative processes are often more flexible and suitable for complex systems and signals with varying levels of noise. In contrast, other techniques employ closed-form solutions that directly compute the result, offering an immediate deconvolution of the signal based on predefined mathematical models. Although closed-form methods may be more efficient in some cases, they can also be more limited when the system's behavior is more complex or less well understood. This section aims to describe the methodologies available in the literature, highlighting their operating principles and unique features. The implemented techniques are applied for the deconvolution of the space charge profiles reported in Fig. 1 and Fig. 2 and compared in order to evaluate their

TABLE I

CLASSIFICATION AND ORDER OF PRESENTATION OF IMPLEMENTED DECONVOLUTION TECHNIQUES.

Type	**Subsection**	**Name**
Frequency Domain	III-A	Fourier Deconvolution
	III-B	Wiener Deconvolution
	III-C	Iterative Blind Deconvolution
Time Domain	III-D	Time Domain Deconvolution
	III-E	Sparse Deconvolution
Hybrid Domain	III-F	Dual Domain Deconvolution
	III-G	STFT Based Deconvolution
	III-H	Laplace Deconvolution

advantages and disadvantages. The results were also compared with those obtained in different papers cited in the present article. For this work authors have chosen to subdivide the techniques according to the domain on which they operate. The classification and order followed are shown in Table I. Below, a comprehensive overview is provided to help identify the most appropriate technique based on the specific applications.

A. Fourier Deconvolution

According the convolution theorem, under certain conditions, the Fourier transform of the convolution between two time domain functions, $x(t)$ and $h(t)$, is equal to the product between the transforms of the functions themselves [17]. Thus, the inverse procedure of convolution, in the frequency domain, is the ratio between the transforms of the two functions. These principles are particularly useful in analyzing Linear Time-Invariant (LTI) systems, allowing both the application of filters to signals and the recovery of original signals. In the case of a PEA measurement, the profile $x(t)$ generated by the application of a voltage pulse is subjected to the convolution product with the response $h(t)$ of the system used for the detection. The convolved profile, $y(t)$, is obtained as output. Neglecting the presence of noise in Eq. 1, to obtain the input profile, deconvolution is performed in the frequency domain according to the following expression [20], [21]:

$$X(j\omega) = \frac{Y(j\omega)}{H(j\omega)} \tag{2}$$

where $X(j\omega)$, $Y(j\omega)$ and $H(j\omega)$ are the Fourier transforms of the quantities $x(t)$, $y(t)$ and $h(t)$. Determining the input signal from the output requires knowledge of the system's transfer function, which in this case corresponds to the PEA cell's response. The main challenge lies in determining $H(j\omega)$, for which different approaches are available in literature. In [22]–[25], the determination of $h(t)$ is performed using the PEA signal that contains only surface charges, without the presence of a space charge, as a calibration signal. According to the origin of the PEA profile, the first peak is generated by the charge distribution at the interface between the dielectric and the outer semiconductive layer, and represents the acoustic wave that reaches the cell almost instantaneously, without undergoing significant attenuation effects. Therefore, the acoustic wave retains its original shape during propagation and can be mathematically approximated as a Dirac delta function, describing a localised distortion-free pulse. Consequently the first peak of the acquired signal can be considered a good approximation of the sensor's impulse response, $H(j\omega)$. In Fig.1 and Fig. 2, the portion of the raw signal extracted for the definition of $H(j\omega)$ is shown highlighted in red. Given the long tail of the impulse response, an interval from the beginning of the signal to just before the second peak is considered. Fig. 3 shows the block diagram for implementing Fourier deconvolution using this approach. In [26], the authors specify that a Dirac pulse cannot be produced in practice, consequently the first peak of the acquired signal cannot be correctly considered as the impulse response of the system. However, knowing the actual characteristics of the applied voltage pulse, it is possible to derive $H(j\omega)$ through an initial deconvolution step between the outer peak of the acquired signal, $y_{ref}(t)$, and a reference signal, $x_{ref}(t)$, with the same characteristics of the applied pulse. In [27]–[29] the reference signal is implemented as a triangular signal or rectangular wave of very short duration, comparable to the width of the outer peak. The process to be implemented can be seen as a two-step deconvolution:

$$H(j\omega) = \frac{Y_{ref}(j\omega)}{X_{ref}(j\omega)} \quad \rightarrow \quad X(j\omega) = \frac{Y(j\omega)}{H(j\omega)} \tag{3}$$

In Fig. 4 a block diagram summarizing the procedure for applying Fourier deconvolution with this second approach is given. Having derived $X(j\omega)$, the profile $x(t)$ can be recovered by the Inverse Fast Fourier Transform (IFFT). The main advantages of deconvolution using Fourier transform include its computational efficiency, especially with the Fast Fourier Transform (FFT) algorithm, and ease of implementation, as it simplifies the deconvolution process through frequency domain division. It also does not require parameters to be adjusted. It is useful for applications in various fields, working with acoustics, imaging and electrical signals, as it effectively restores blurred

or distorted signals when the transfer function of the system is known. However, there are some aspects to be taken into account that can affect the final result. Deconvolution in the frequency domain can amplify noise, especially at high frequencies, leading to unstable results. In fact, if the presence of noise is taken into account, the Eq. 2 becomes:

$$X(j\omega) = \frac{Y(j\omega)}{H(j\omega)} - \frac{N(j\omega)}{H(j\omega)} \tag{4}$$

where divisions by zero or very close to zero can occur. Small spectral values can cause singularities, and aliasing of the data can introduce artifacts when working with non-periodic signals, such as when processing a space charge profile. Applying a low-pass filter helps mitigate this by attenuating the high-frequency noise, stabilizing the output, and improving the Signal-to-Noise Ratio (SNR). However, this introduces a trade-off: too much filtering can remove important signal details, while insufficient filtering may not effectively reduce the noise. Fig. 5 shows the result of deconvolution by Fourier transform of the PEA signal obtained with model cable. Specifically, the deconvolved profile (blue) and the deconvolved and filtered profile (red) are shown. As expected, the deconvolved profile shows a considerable reduction in the SNR, which makes the second peak unrecognizable. The use of a low-pass filter is therefore essential to eliminate the high-frequency components. However, with the filtered signal, the main problem emerges, namely baseline distortion. This is more evident in Fig. 6 that shows the result of Fourier deconvolution of the PEA profile for full-size cable. Once again, a low SNR signal and a filtered signal with baseline distortions can be observed. Basically, Fourier deconvolution applied to the PEA signals for both cables, model and full size, showed a significant reduction in SNR, making it difficult to identify profile details. This phenomenon has been observed in both configurations, suggesting that the limitations encountered are intrinsic to the Fourier deconvolution method rather than related to the size of the cables used. A possible explanation for this behavior is the width of the acquired temporal window. A larger window, one that includes the tail of the second peak up to its natural convergence towards zero, would avoid the introduction of artifacts during the transition to the frequency domain, making the result more stable. In general, this technique is suitable for applications where signals with high SNR are acquired. These results are in agreement with what can be found in the literature, confirming the validity of the observations reported in previous studies and supporting the reliability of the current analysis.

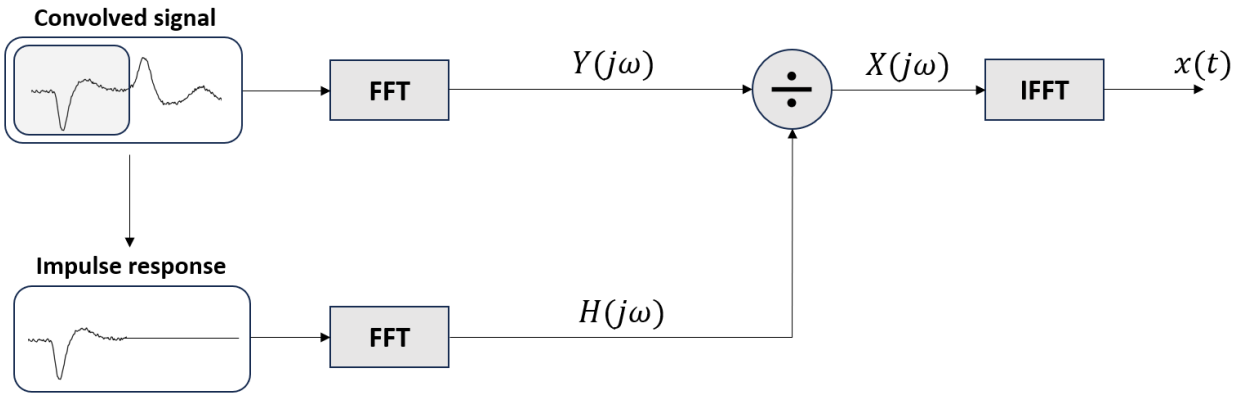

Fig. 3. Block diagram for the implementation of Fourier deconvolution. Method 1.

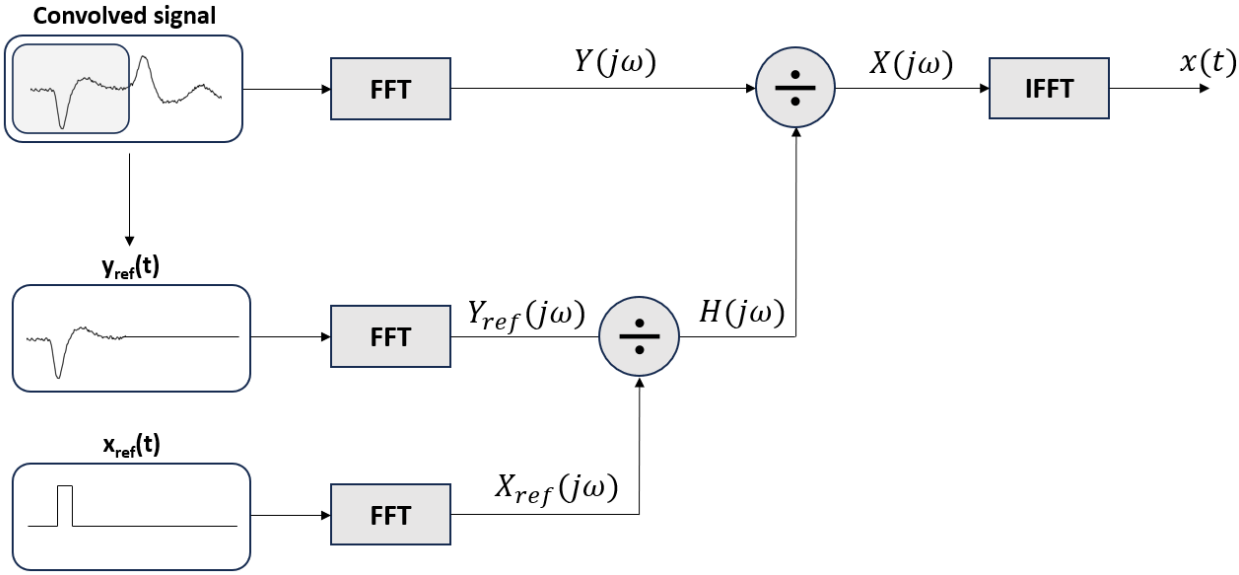

Fig. 4. Block diagram for the implementation of Fourier deconvolution. Method 2.

B. *Wiener Deconvolution*

If the source of noise is known or in general there is enough information to be able to define a statistical model for estimating the noise, it is possible to implement deconvolution using a Wiener filter as reported in [30]–[32]. Wiener deconvolution enables simultaneous noise suppression and signal recovery, operating exclusively in the frequency domain and it can be seen as a modified version of Fourier deconvolution. While both techniques aim to recover a signal from a degraded version, Wiener deconvolution incorporates statistical information about the noise and the original signal, leading to improved results in the presence of noise. In contrast, Fourier deconvolution primarily focuses on the frequency domain without explicitly considering the noise characteristics. The reference equation is as follows:

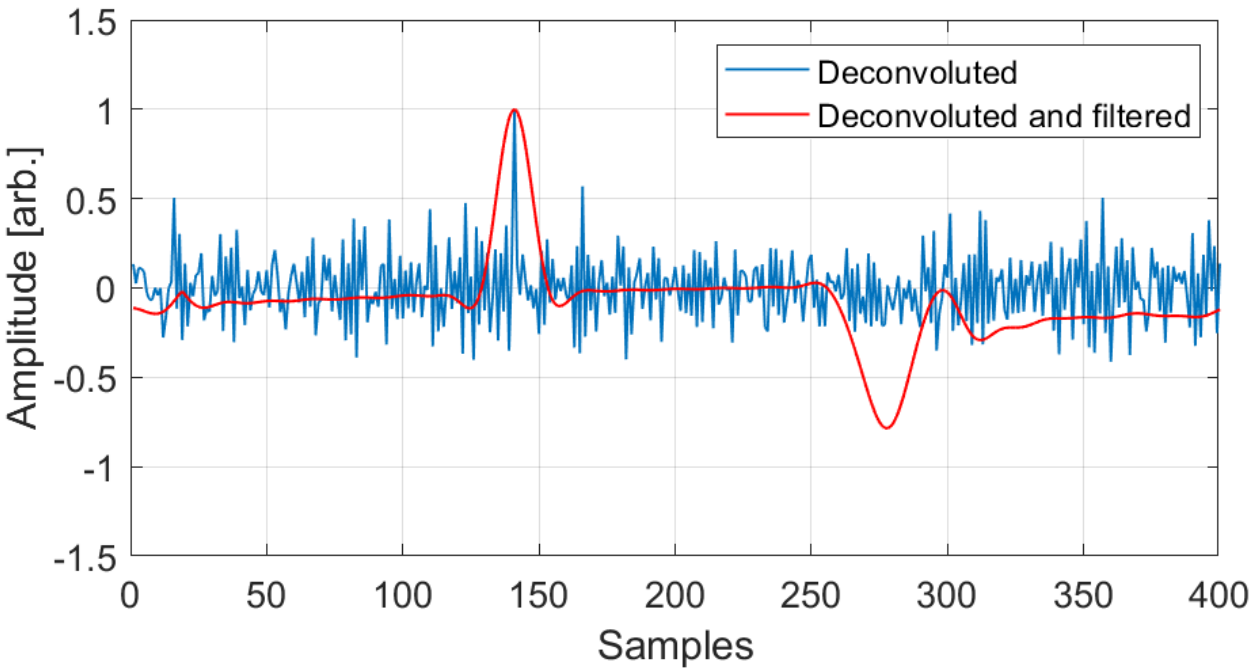

Fig. 5. Deconvolved model cable profile with Fourier deconvolution.

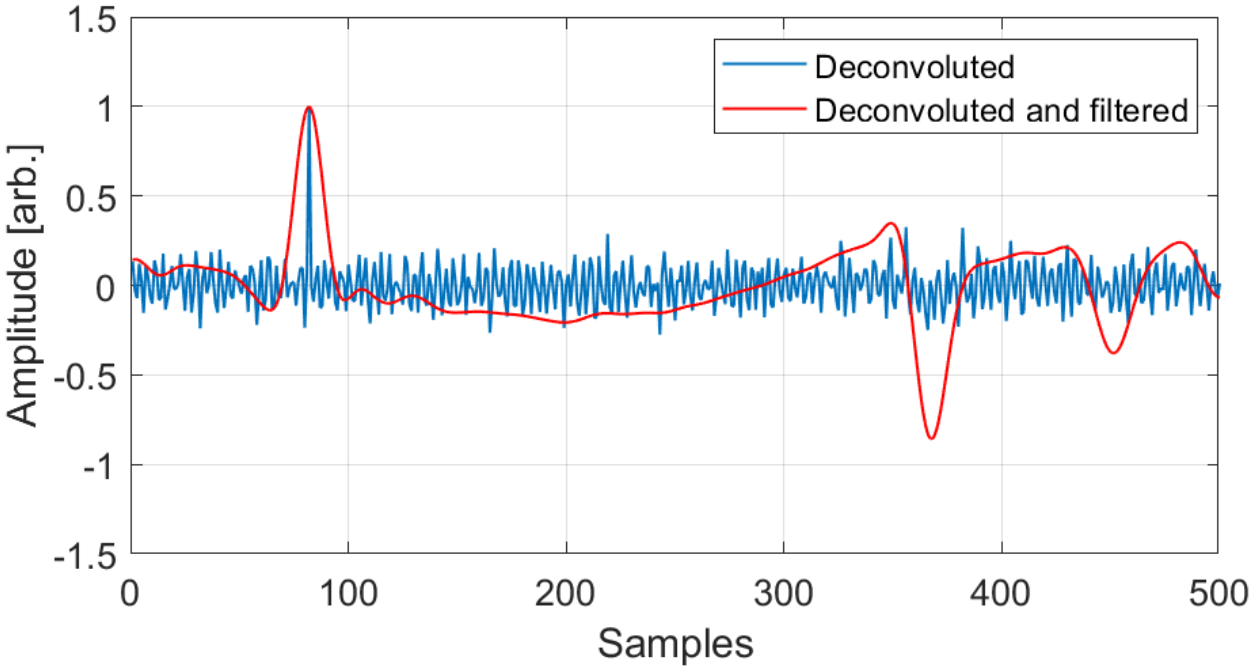

Fig. 6. Deconvolved full-size cable profile with Fourier deconvolution.

$$X(j\omega) = W(j\omega) \cdot Y(j\omega) \tag{5}$$

Where $W(j\omega)$ is the Wiener filter represented by the following expression:

$$W(j\omega) = \frac{H^*(j\omega)}{|H(j\omega)|^2 + k \cdot SNR} \tag{6}$$

where $|\cdot|$ and $*$ are the modulus and conjugate operators and k an adjustment parameter of the filter. It can be seen that for k tending to zero $W(j\omega)$ reduces to $\frac{1}{H(j\omega)}$. In this case, Wiener deconvolution is equal to Fourier deconvolution. In real world scenarios, the exact power spectra of the noise are rarely known. To address this issue, a regularization parameter, γ_W, is introduced, serving as an approximation of the SNR and stabilizing the deconvolution process in the presence of noise. The expression of the transfer function becomes:

$$W(j\omega) = \frac{H^*(j\omega)}{|H(j\omega)|^2 + \gamma_W} \tag{7}$$

Here, γ_W acts as a regularization factor that approximates the ratio between the noise and signal power spectra. This structure helps to prevent the amplification of noise in the frequencies where the function $H(j\omega)$ has very small or zero values, which would otherwise lead to instability in the deconvolution process. By adjusting γ_W, the balance between noise reduction and signal restoration can be controlled, even in cases where no precise noise model is available. In Fig. 7

a block diagram summarizing the procedure to implement Wiener deconvolution is given. Since the way of $H(j\omega)$ determination has not changed, the diagram is similar to Fig. 3 with only the Wiener filter application part added (dashed red line).

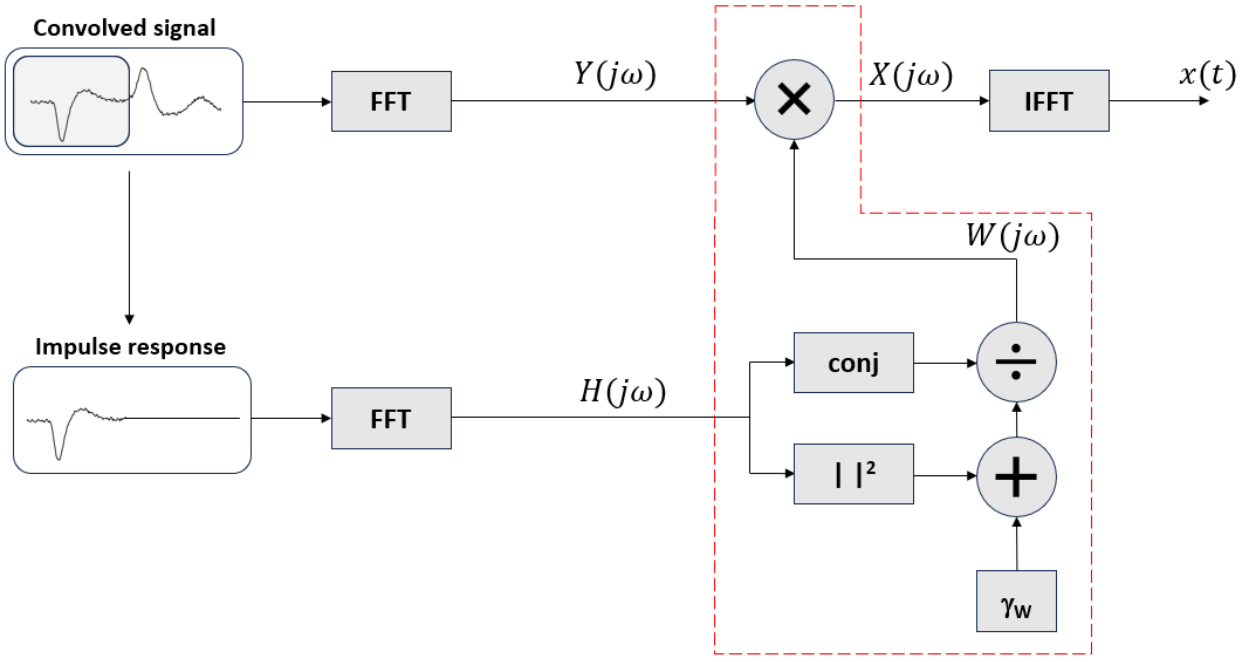

Fig. 7. Block diagram for the implementation of Wiener deconvolution.

Fig. 8 shows the results of Wiener deconvolution applied to model cable profile, with varying values of the parameter γ_W, which likely controls the regularization or noise suppression in the deconvolution process. The plot shows three lines, each obtained with a different γ_W value. As γ_W increases, the signal becomes smoother, indicating that higher γ_W values lead to stronger noise suppression, but possibly at the cost of some signal detail. In particular, as with Fourier deconvolution, there is a baseline distortion that is accentuated as γ_W increases. A similar result is obtained for the deconvolution of the full-size cable profile, as shown in Fig. 9. These results agree with the findings of [33], where a detailed analysis is presented for the optimal estimation of the parameter γ_W, which is essential for the deconvolution of signals affected by noise. The authors propose an analytical approach to determine the critical value that minimises the distortion of the reconstructed signal. The formulation is based on considerations of sampling frequency and system dynamics. In summary, Wiener deconvolution allows the reconstruction of the input signal by preventing the amplification of noise. The technique is an extension of Fourier

deconvolution that incorporates a denoising effect. It is therefore not surprising that the result does not differ from that obtained by Fourier deconvolution with low-pass filter application. It performs better than simple inverse filtering for signals with noise, especially when the SNR is low. There remains the problem of baseline distortion due to inadequate distribution of the low-frequency components. Furthermore, the introduction of a regularization parameter introduces a trade-off between good signal filtering and low sensitivity within a certain frequency range, which could lead to significant information loss.

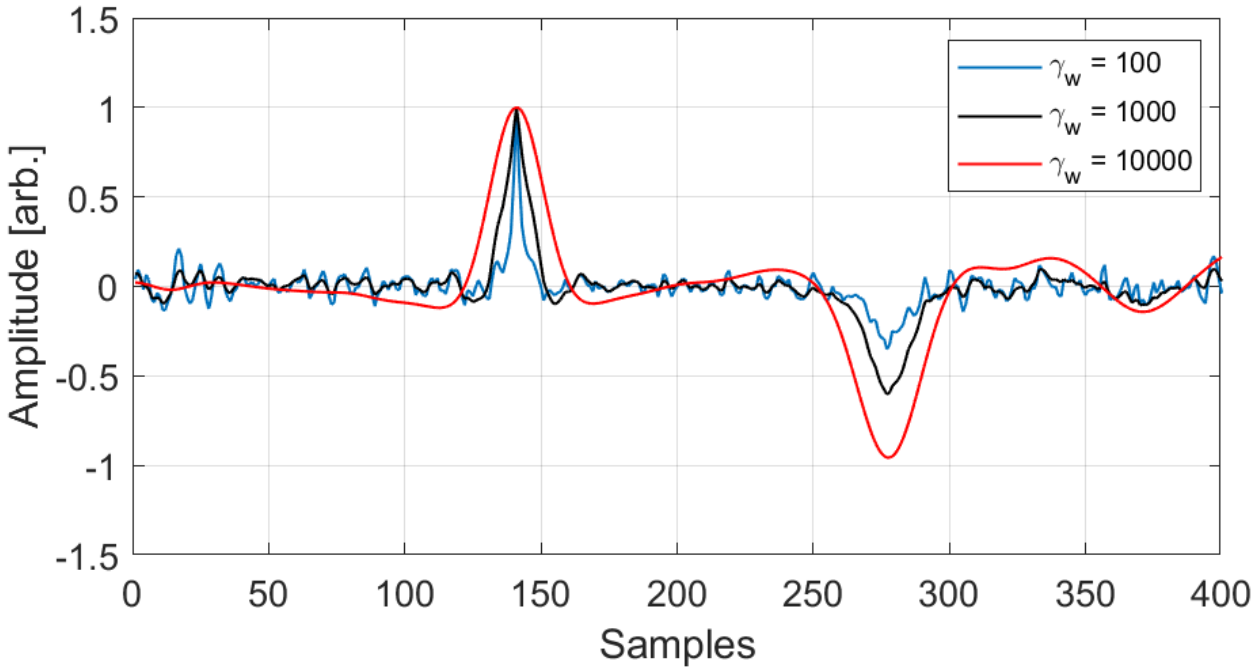

Fig. 8. Deconvolved model cable profile with Wiener deconvolution.

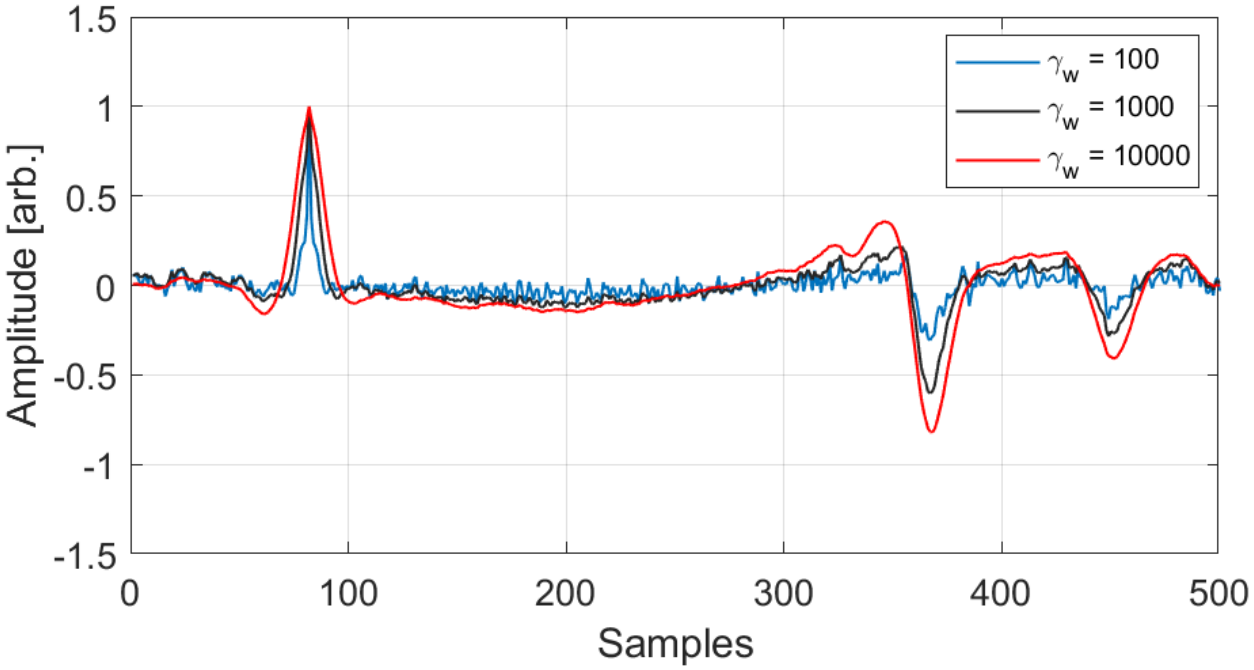

Fig. 9. Deconvolved full-size cable profile with Wiener deconvolution.

C. Iterative Blind Deconvolution

In [34] and [35], an iterative deconvolution technique is presented for image processing, while in [36] the same technique is applied for the deconvolution of a PEA profile, adapting it for signal processing. The Iterative Blind Deconvolution (IBD) is an algorithm used to estimate both the deconvolved signal and the system response, without requiring prior knowledge of either. This is particularly useful when the system characteristics are unknown or difficult to model. The procedure begins with initial estimates for the input signal, $x_0(t)$, and the function, $h_0(t)$. The iterative process then alternates between updating these estimates until a convergence criterion is satisfied. This process can be divided into three main steps: first, the estimation of the system response $h_k(t)$, second, the update of the input signal $x_k(t)$, and third, the loop exit condition check. The convergence criterion can be defined in several ways, such as by minimizing noise or maximizing the SNR of the deconvolved signal. Alternatively, a cost function to minimize, such as the Mean Square Error (MSE) of the estimated signal, can be used. In addition to the initial estimates the algorithm requires a tolerance value, ϵ, for the loop exit condition. The update at the k-th iteration is implemented with the following equations:

$$H_k(j\omega) = \frac{Y(j\omega)X^*_{k-1}(j\omega)}{|X_{k-1}(j\omega)|^2 + \frac{\alpha}{|H_{k-1}(j\omega)|^2}} \tag{8}$$

$$X_k(j\omega) = \frac{Y(j\omega)H_k^*(j\omega)}{|H_k(j\omega)|^2 + \frac{\alpha}{|X_{k-1}(j\omega)|^2}} \tag{9}$$

where the capital letters indicate the Fourier transforms. The parameter α is a constant with values between 0 and 1, used to account for the noise level. From equations 8 and 9, it can be observed that the technique is an iterative application of a Wiener filter. The IBD technique is inherently characterized by the non-uniqueness of its solution, as different combinations of $h(t)$ and $x(t)$ can satisfy the criteria defined by the algorithm. This ambiguity makes the reliability of the solution uncertain, as the final outcome heavily depends on the initial assumptions $x_0(t)$ and $h_0(t)$. Consequently, to narrow the solution space and guide the algorithm toward a more realistically plausible solution, it's necessary to introduce constraints on the impulse response or the deconvolved signal. This implies accurate knowledge of measurement conditions, material properties, and system physics. Despite these limitations, the technique offers some significant advantages. These include low computational complexity compared to more sophisticated approaches and the integration of Wiener filters in the iterative process, which prevents noise amplification. This ensures the convergence of the iterative loop, leading to a stable and robust estimation of both the signal and the impulse response, even in the presence of noise.

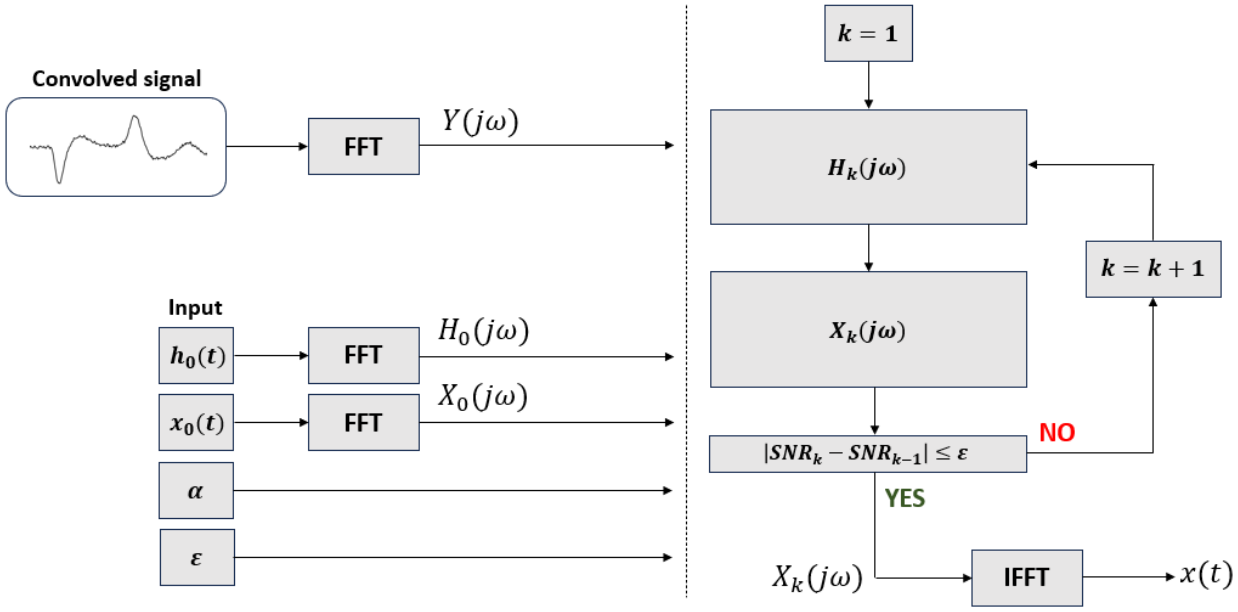

Fig. 10. Block diagram for the implementation of IBD.

In Fig. 10, the block diagram for the implementation of the IBD is presented. As suggested

in [36], the initial estimate of the original signal can be a profile with two unitary peaks, while the initial estimate of the system response has been considered as a damped sinusoidal function. In Fig. 11 and 12, the results obtained with the signals for the model and full-size cables are presented. The technique successfully provides a deconvolved signal without baseline distortion. It's worth noting the absence of the reflected signal from the conductor, as in the initial assumption, $x_0(t)$, only two acoustic sources are considered at the inner and outer radius. A low-pass filter was applied to further smooth the signal and eliminate the presence of high-frequency components. The results obtained are in agreement with those reported in [36].

D. Time Domain Deconvolution

The previously discussed techniques operate in the frequency domain. However, the same problem can be addressed in the time domain [23], [37]–[39]. Considering Eq. 1 in discrete form, it is possible to express the problem with a matrix notation:

$$\mathbf{y} = \mathbf{H} * \mathbf{x} + \mathbf{n} \tag{10}$$

where $\mathbf{H}$ is the system response or convolution matrix. The latter, also known as Toeplitz matrix, is constructed based on the impulse response function $h(t)$. Its structure reflects the time-dependent nature of the convolution process, where each row represents a shifted version of $h(t)$ as shown in the following example in the case of n samples:

$$\mathbf{H} = \begin{pmatrix} h(t_0) & h(t_1) & h(t_2) & ... & h(t_n) \\ h(t_n) & h(t_0) & h(t_1) & ... & h(t_{n-1}) \\ h(t_{n-1}) & h(t_n) & h(t_0) & ... & h(t_{n-2}) \\ : & : & : & ... & : \\ h(t_1) & h(t_2) & h(t_3) & ... & h(t_0) \end{pmatrix} \tag{11}$$

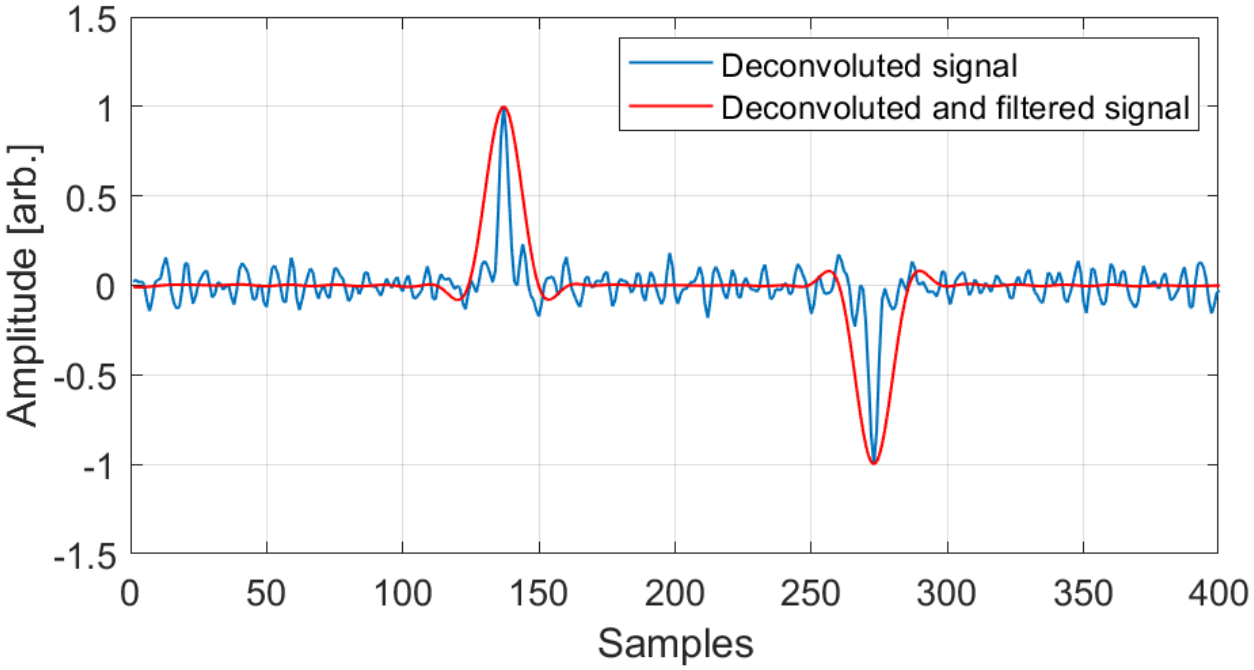

Fig. 11. Deconvolved model cable profile with IBD.

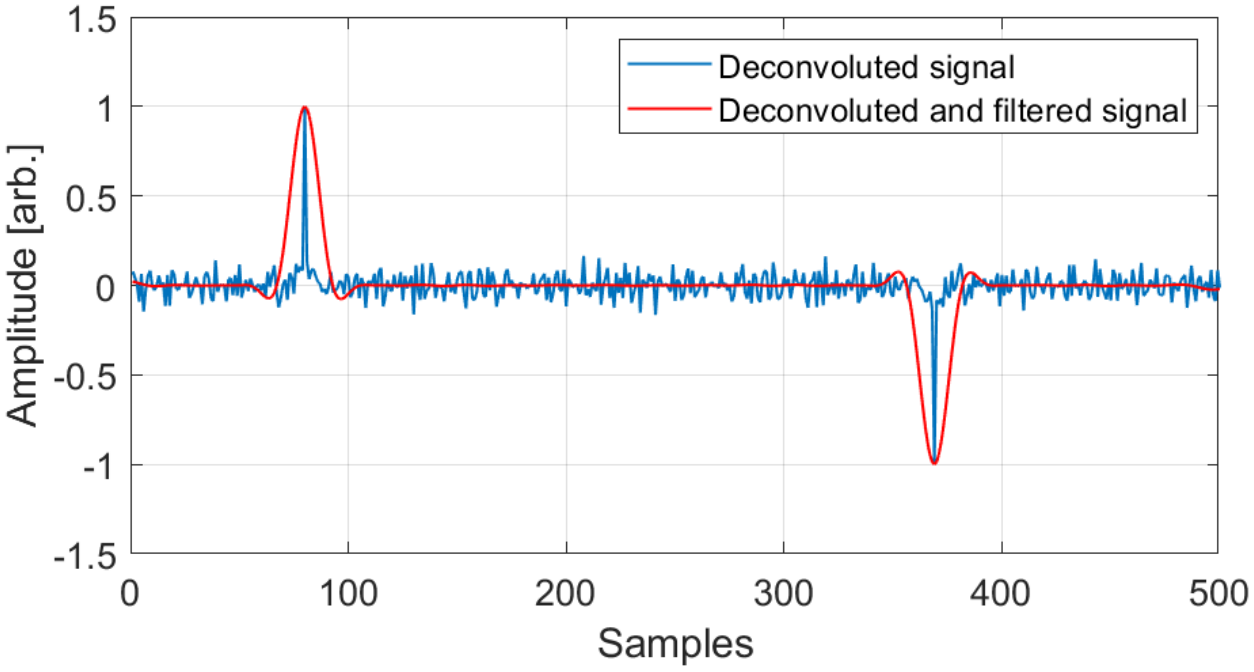

Fig. 12. Deconvolved full-size cable profile with IBD.

A direct solution by inverting **H** is not feasible due to two main issues: noise amplification and the almost-singular nature of **H**, which results in an ill-conditioned problem with a determinant

close to zero [40]. To overcome these challenges, an estimate of $\mathbf{x}$ is obtained using regression methods, such as the Least Squares Error (LSE) method. This approach involves minimizing a cost function, defined as:

$$J_{TD}(\mathbf{x}) = ||\mathbf{y} - \mathbf{H}\mathbf{x}||_2^2 + \lambda_{TD}||\mathbf{x}||_2^2 \tag{12}$$

where $||\cdot||_2$ is the ℓ_2 norm functions, while λ_{TD} is a regularization parameter. The cost function consists of two terms: an estimation error term and a regularization term, the latter is introduced to improve stability, given the ill-conditioned nature of the problem. This technique is known as Tikhonov regularization. The cost function defined in this way is convex and the closed-form solution that minimises J_{TD} can be expressed by the following relations:

$$\mathbf{x} = (\mathbf{H}^T\mathbf{H} + \lambda_{TD}\mathbf{I})^{-1}\mathbf{H}^T\mathbf{y} \tag{13}$$

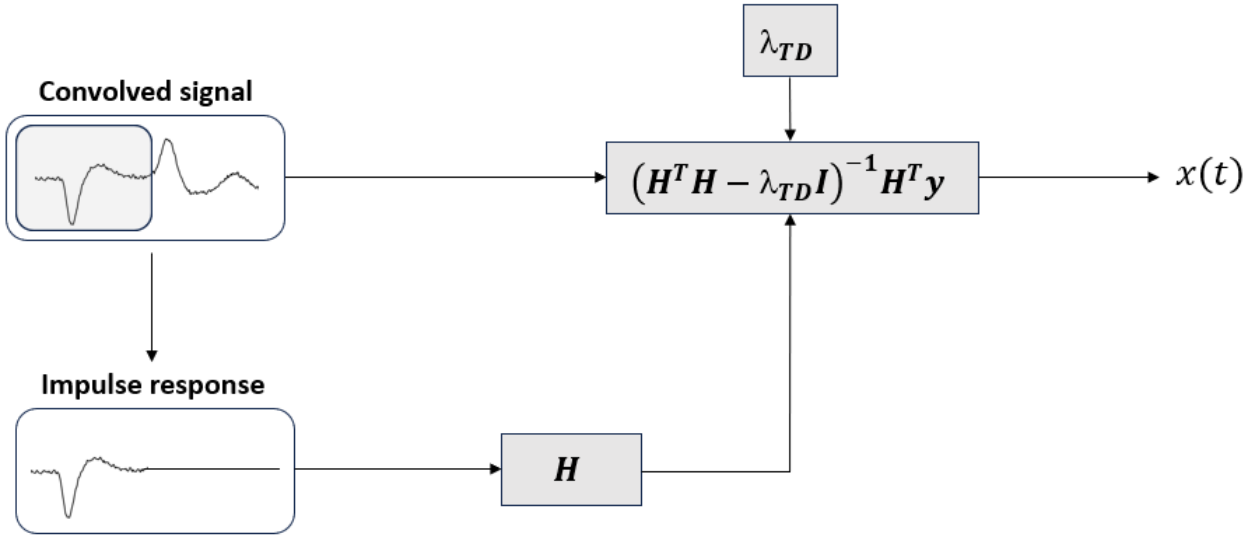

Fig. 13. Block diagram for the implementation of time domain deconvolution.

where $\mathbf{I}$ is the identity matrix. The estimation therefore depends on the measured profile, the $\mathbf{H}$ matrix and the parameter governing the stability and accuracy of the solution. The optimal λ_{TD} value can be assessed by applying the L-curve method [40]. Fig. 13 shows the diagram for the implementation of time domain deconvolution while Fig. 14 and Fig. 15 show the results obtained, with different λ_{TD} values, for the model and full-size cable profiles, respectively. For low λ_{TD} values, the effect of regularisation is attenuated, leading to lower stability in the solution. As λ_{TD} increases, an improvement in the process is observed, providing profiles with

reduced noise content and no spurious low-frequency components causing baseline distortion. However, if the regularization parameter is too large, the resulting solution becomes excessively smooth, leading to a loss of detail. In this case, the model prioritizes stability at the expense of accuracy, introducing a high bias and making the solution less representative of the physical reality of the problem. The results obtained are in agreement with those reported in [37], [38]. Time domain deconvolution proves to be a robust and accurate option for dealing with scenarios where signal distortion is dominant. Although it provides a solution with a reduced content of spurious low-frequencies, the approach is computationally very expensive. Indeed, the calculation time is highly dependent on the size of the H matrix. Furthermore, the problem is inherently ill-conditioned and requires an estimation technique (LSE) to obtain a result. The estimation, however, can be unstable and requires a regularisation technique to guarantee the stability of the solution. To obtain the optimal value of the regularisation parameter, an additional technique such as L-curve analysis can be employed. However, all of these interconnected steps make the process complex and computationally demanding, significantly increasing the execution time and the difficulty of handling the parameters.

E. Sparse Deconvolution

Among the several deconvolution techniques employed in signal recovery for PEA measurement, sparse deconvolution stands out for its effectiveness in handling signals with sparse characteristics, such as those occurring at material interfaces or within small localized regions, offering superior noise suppression and resolution compared to traditional approaches [41]. This technique is based on the assumption that the signal to be estimated, $x(t)$, possesses an inherently sparse structure, which means that most of its values are zero or close to zero, with only a few significant components concentrated in specific locations. As well as the previous one, it is a technique applied in the time domain in which the solution is derived by imposing a sparsity constraint on the signal **x**. This is reflected in the regularization term added to the cost function, J_{SD}, defined by the following relationship:

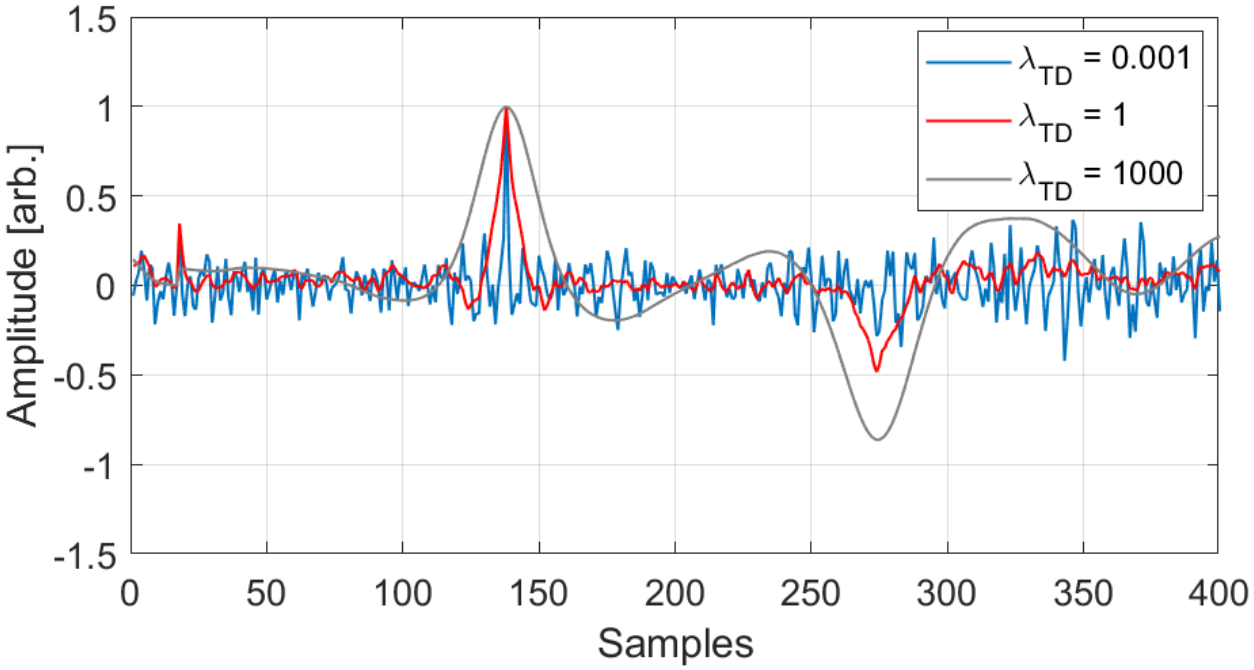

Fig. 14. Deconvolved model cable profile with time domain deconvolution.

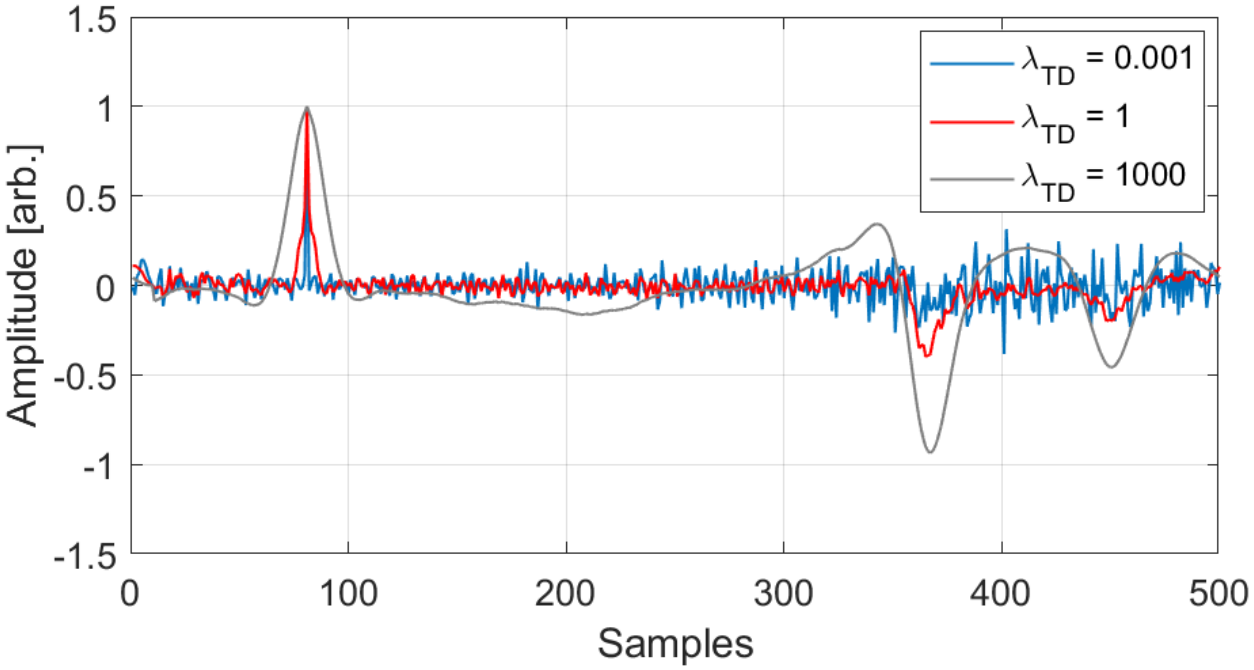

Fig. 15. Deconvolved full-size cable profile with time domain deconvolution.

$$J_{SD}(\mathbf{x}) = \frac{1}{2}||\mathbf{y} - \mathbf{H}\mathbf{x}||_2^2 + \lambda_{SD}||\mathbf{x}||_1 \tag{14}$$

where $||\cdot||_1$, the ℓ_1 norm function, is considered for the regularization term, unlike Eq. 12. This constraint forces many signal values toward zero, promoting sparsity. The parameter λ_{SD} is used to adjust the trade-off between data fidelity and sparsity. Low λ_{SD} values give greater weight to error minimisation, whereas increasing λ_{SD} values give greater weight to signal sparsity. However, in contrast to the cost function J_{TD}, the $||\mathbf{x}||_1$ term of J_{SD} is not differentiable everywhere and thus does not present a closed solution for the identification of the minimum. For this reason, an iterative approach to solving the problem is necessary. The cost function thus defined turns out to be convex, thus ensuring that the optimisation process will be simple, as there will be no local minima that could trap the algorithm. In [41], the approach used to find the solution is the Majorization-Minimisation (MM) algorithm [42]. It is an iterative method whose principle is to replace the original problem with a 'greater' problem that is easier to solve at each iteration, and then minimise that greater function. Specifically, the new function $G(\mathbf{x})$ must satisfy the following conditions:

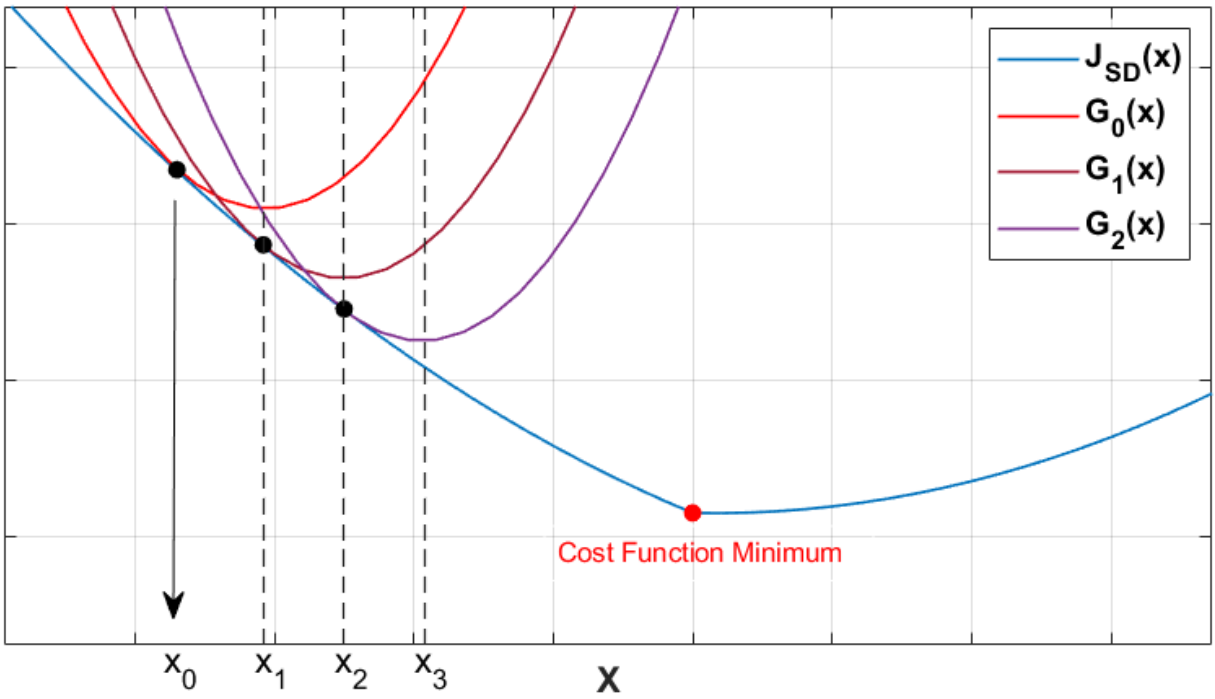

Fig. 16. 1-D example for the MM algorithm.

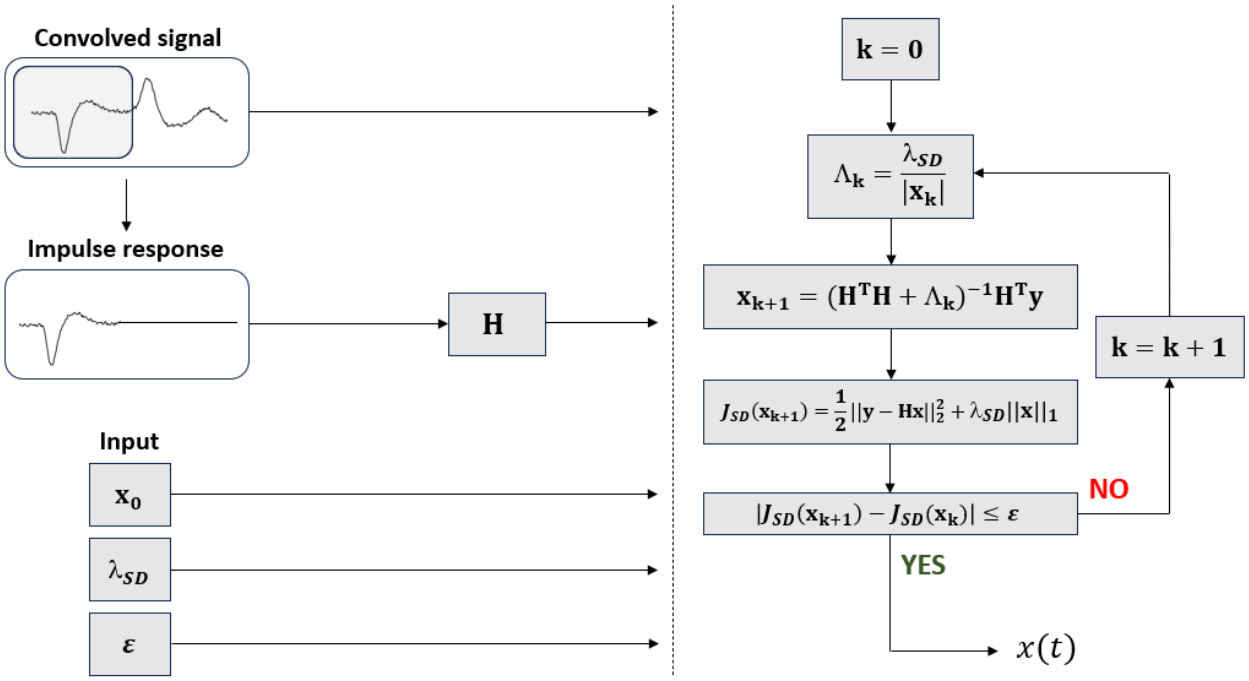

Fig. 17. Block diagram for the implementation of sparse deconvolution.

$$G(\mathbf{x}) \geq J_{SD}(\mathbf{x}) \quad ; \quad G(\mathbf{x}_k) = J_{SD}(\mathbf{x}_k) \tag{15}$$

The latter indicates that the function $G(\mathbf{x})$ must always be greater than $J_{SD}(\mathbf{x})$ and have one point in common with it. The first common point is established by providing an initial estimate of the deconvolved signal, $\mathbf{x}_0$. Then the function $G(\mathbf{x})$ is updated so that the new common point coincides with the minimum of the previous one. The iterative procedure continues until the minimum of function $G_k(\mathbf{x})$ coincides with the minimum of function $J_{SD}(\mathbf{x})$. The equations used for the update are:

$$G_k(\mathbf{x}) = \frac{1}{2}||\mathbf{y} - \mathbf{H}\mathbf{x}||_2^2 + \frac{1}{2}\mathbf{x}^T\Lambda_k\mathbf{x} + \frac{\lambda}{2}||\mathbf{x}_k||_1 \tag{16}$$

$$\mathbf{x}_{k+1} = (\mathbf{H}^T\mathbf{H} + \Lambda_k)^{-1}\mathbf{H}^T\mathbf{y} \tag{17}$$

where Λ_k is a diagonal matrix with elements of $\lambda_{SD}/|\mathbf{x}_k|$ on the diagonal. A graphic example of the iterative process, in the one-dimensional case, is shown in Fig. 16. In addition to the initial estimate, $\mathbf{x}_0$, the algorithm requires a maximum number of iterations and a tolerance, ϵ, for the exit condition, evaluated as follows:

$$|J_{SD}(\mathbf{x}_{k+1}) - J_{SD}(\mathbf{x}_k)| < \epsilon \tag{18}$$

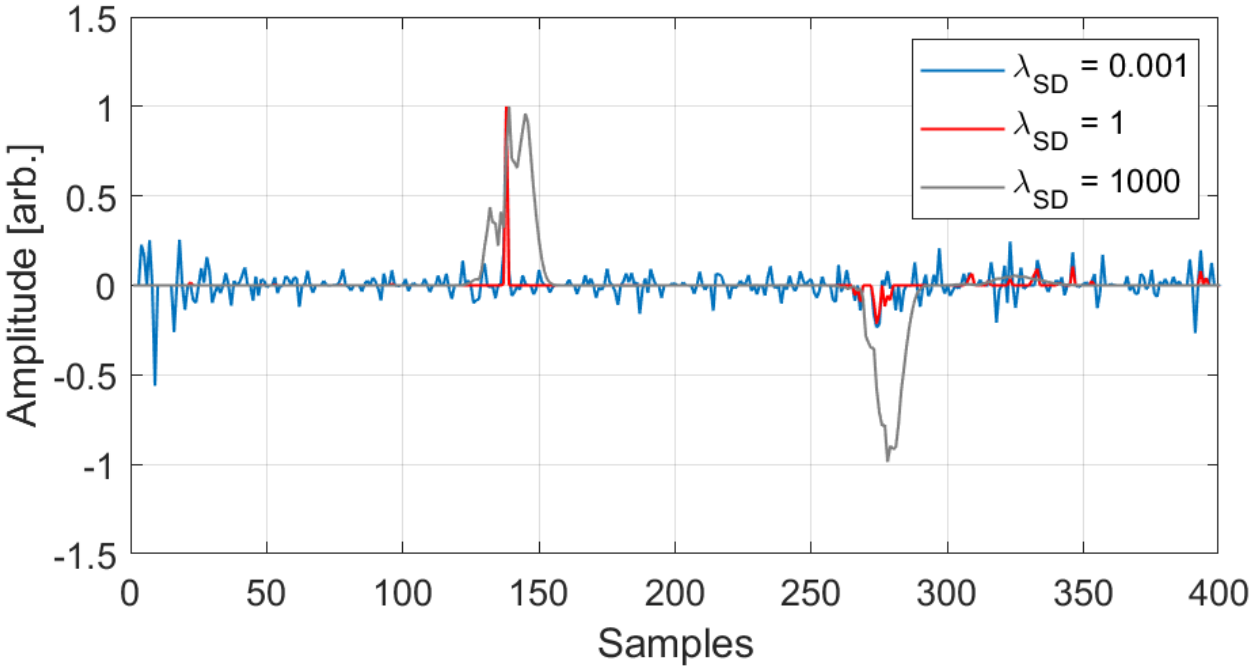

Fig. 18. Deconvolved model cable profile with sparse deconvolution.

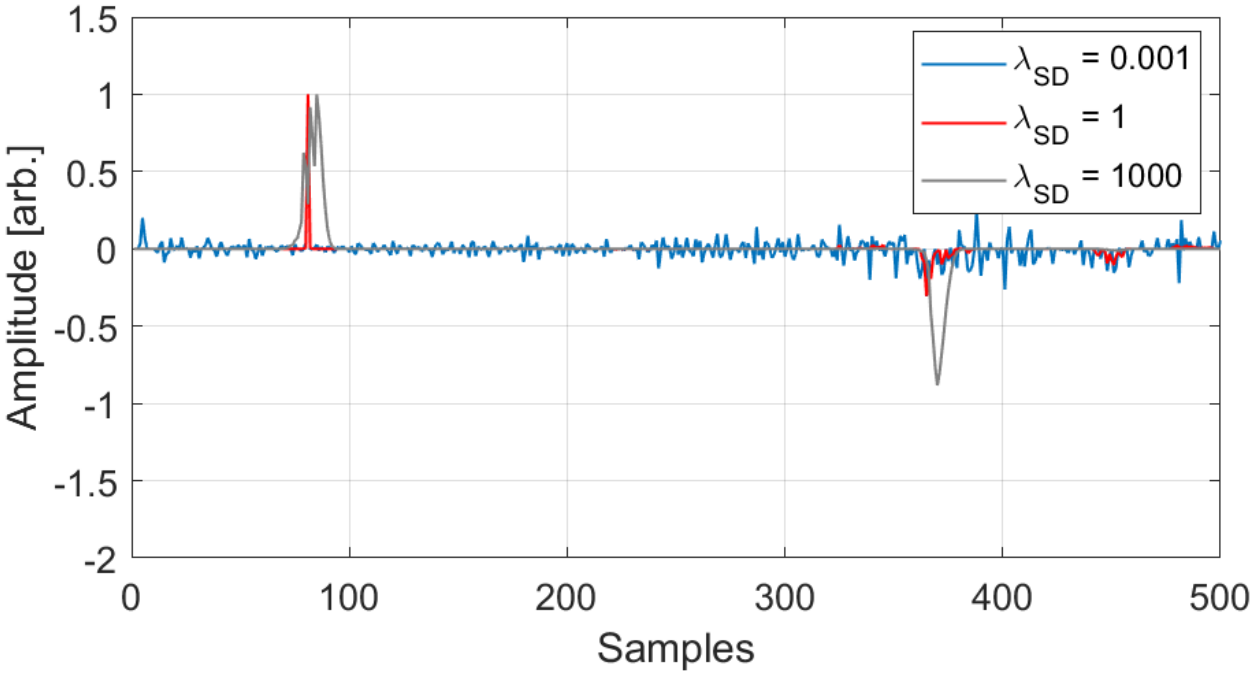

Fig. 19. Deconvolved full-size cable profile with sparse deconvolution.

Fig. 17 shows a block diagram of the iterative process for implementing sparse deconvolution. Fig. 18 and Fig. 19 show the results of applying sparse deconvolution to the PEA profiles obtained

for model and full-size cables. Again, different profiles are shown as the regularization parameter changes. For small values of λ_{SD}, a reduced effect of regularisation is observed, with the signal clearly covered by noise, although a tendency towards sparse solution can be seen. As λ_{SD} increases, a reduced noise content is observed as well as a noticeable increase in resolution (red curve). However, there is also a reduction in the second peak compared to the first. As with IBD, the absence of the reflection is due to the assumption of two single acoustic sources in the initial estimation, $\mathbf{x}_0$. The results obtained are in agreement with those reported in [41]. However, by continuing to increase λ_{SD}, two effects are observed. The first is an increase in the second peak and the other is a reduction in resolution. It is believed that forcing the sparsity of the signal leads to a greater penalty on small values, which suppresses the noise and redistributes the energy on the main peaks. Since the technique is based on obtaining a sparse solution, this effect can be seen as undesirable. Sparse deconvolution is suitable for analyzing signals with well-defined peaks, such as those occurring at material boundaries or in thin regions of charge accumulation. The main fields of application can be measurements on flat specimens, with thin thickness or in the case of multilayer specimens where high resolution is required both instrumentally and in processing. Alternatively, as suggested in [41], the technique is suitable for evaluating the presence of micro bills in dielectric materials due to the high resolution that can be achieved. Furthermore, due to the sparsity constraint, this technique is able to effectively suppress noise, reducing spurious components without compromising the quality of meaningful information. Unlike other techniques, sparse deconvolution also minimises baseline distortion, improving the accuracy of the reconstructed signal and reducing artifacts introduced by high-frequency amplification. However, this technique has some limitations that complicate its use. One is the choice of the regularization parameter, which determines the trade-off between signal resolution and sparsity imposition. This makes it necessary to use optimization strategies to find the most suitable value. Gholami et al. proposed an efficient approach using Generalized Cross-Validation (GCV) to determine the optimal value avoiding long and costly empirical tests [43]. Furthermore, since the sparse deconvolution cost function is not everywhere differentiable, there is no closed solution to the problem. Consequently, it is necessary to resort to iterative algorithms that increase the computational cost compared to simpler techniques.

F. Dual Domain Deconvolution

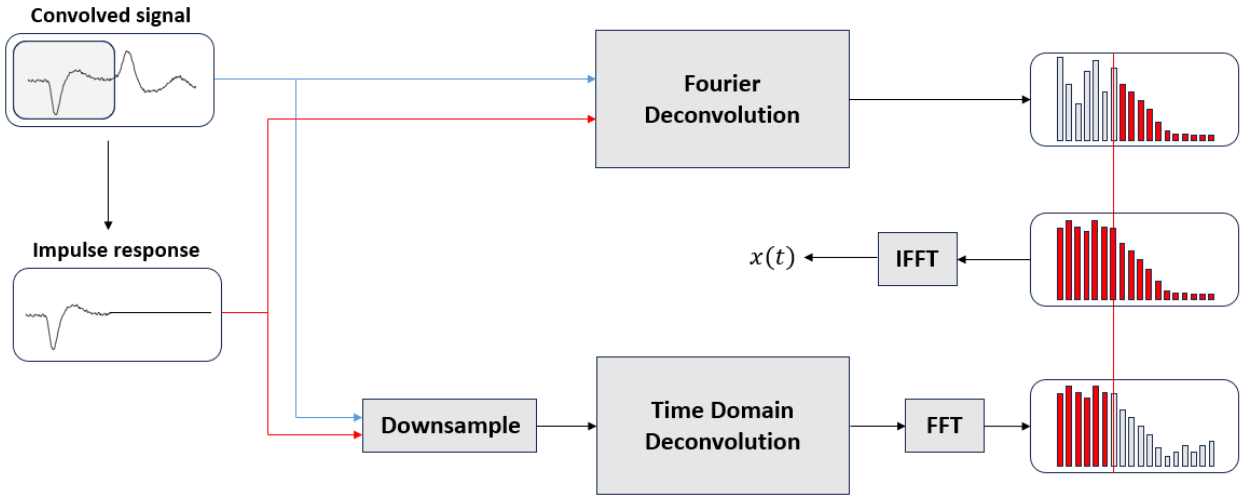

Fig. 20. Block diagram for the implementation of dual domain deconvolution.

Conventional approaches, such as Fourier deconvolution, are prone to instability in low-frequency spectral components. On the other hand, deconvolution in time domain, while less affected by these issues, is computationally more demanding, particularly for signals with a great number of samples or in real-time analysis. To address these limitations, a dual domain deconvolution has been developed by Prastika et al., leveraging the strengths of both techniques [44]–[47]. This technique reconstructs the deconvolved signal by merging signal spectral components obtained through deconvolution performed in the time and frequency domains. Specifically, the first (time) provides low-frequency content linked to a signal with an undistorted baseline, while the second (frequency) provides high-frequency content from a signal with a greater SNR. To further reduce the computational cost of time domain deconvolution, the signal is first downsampled to reduce the data size. The results are then merged to produce a comprehensive signal free from high frequency spectral noise and baseline distortions. A diagram for the implementation of dual domain deconvolution is shown in Fig. 20, which refers to the diagrams shown in Fig. 3 and Fig. 13 for the implementation of the individual techniques.

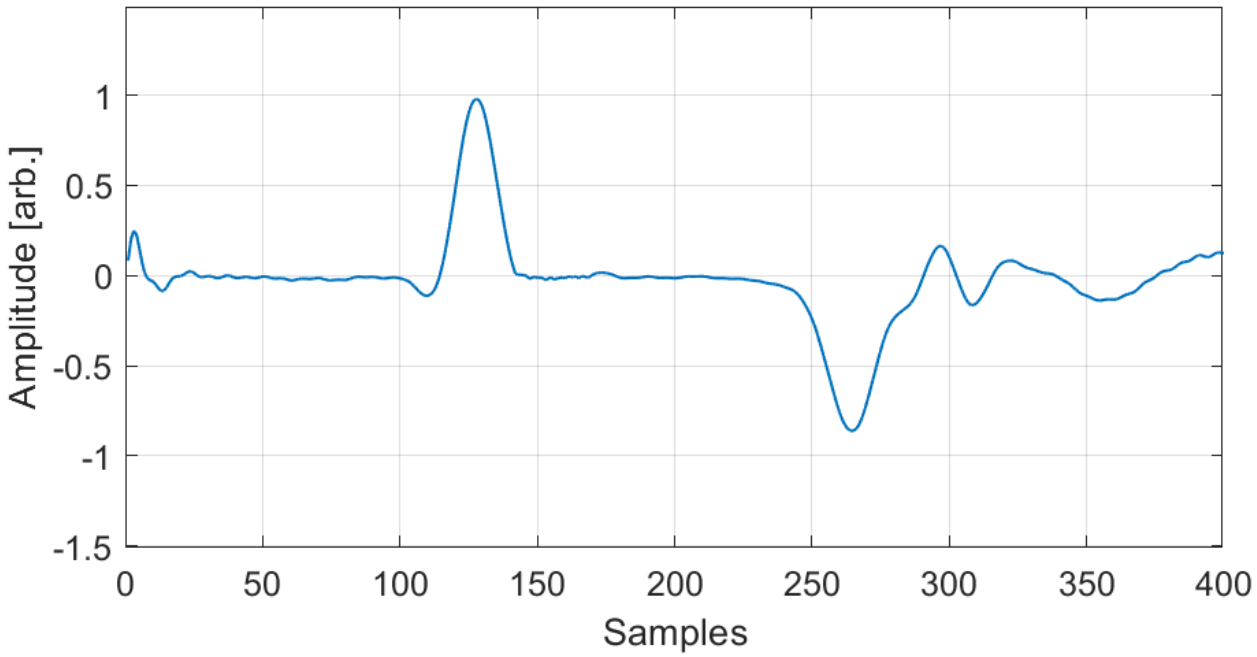

Fig. 21. Deconvolved model cable profile with dual domain method.

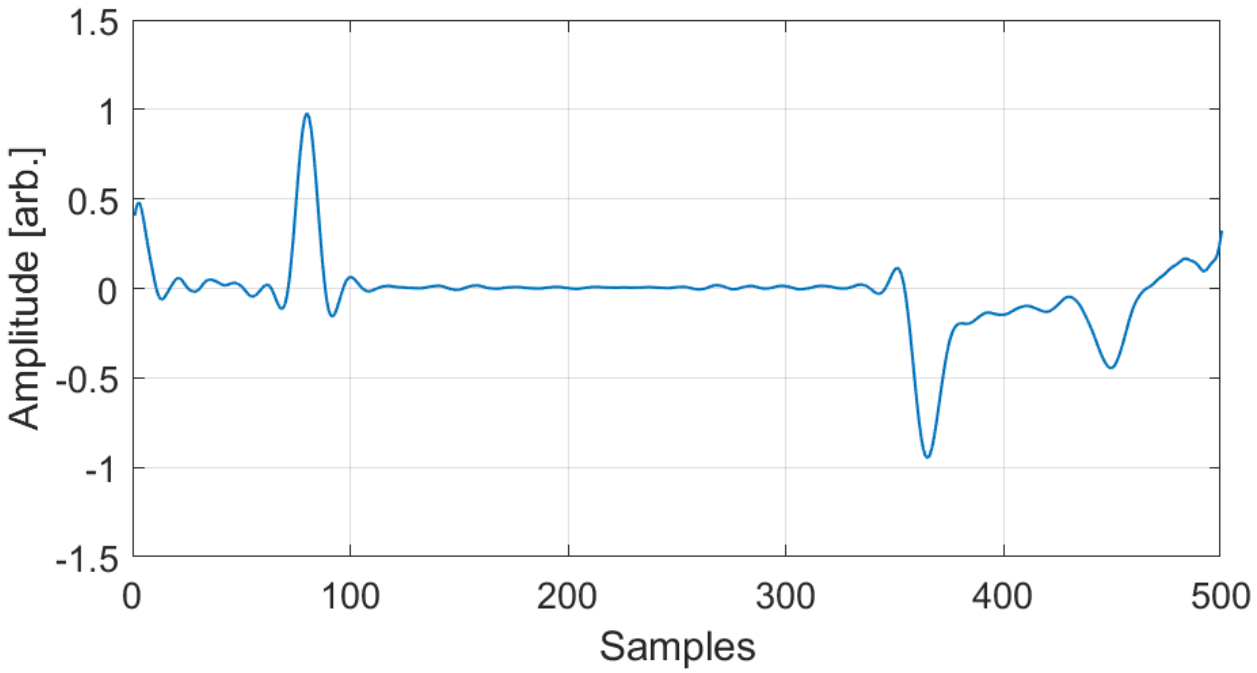

Fig. 22. Deconvolved full-size cable profile with dual domain method.

For downsampling, an averaging technique is used. This is a method in which the value of each sample in the downsampled signal is obtained by averaging a group of adjacent samples

from the original signal. This process reduces the resolution of the signal by decreasing the amount of data required to represent it, but can result in a loss of detail and smoothing of rapid variations. In spectral terms, when downsampling is performed, the signal is sampled at a lower frequency, which implies that the higher frequencies present in the original signal may not be represented correctly. However, since only the low-frequency components are extracted from the signal obtained by deconvolution performed in the time domain, this loss of information is accepted as it leads to a reduction in calculation time. Another important aspect, emphasized in [45], is the choice of appropriate criteria to overlap the two portions of the spectrum. Fig. 21 and Fig. 22 show the profiles deconvolved by dual deconvolution for model and full-size cables respectively. Both profiles show a significant improvement in signal reconstruction compared to techniques based only on time or frequency domain. Analysis of the results shows a reduction in baseline distortions, typically present in Fourier deconvolution, and an improved SNR compared to time deconvolution. However, the quality of the reconstruction strongly depends on the fusion criteria between the two domains, in particular the choice of the transition frequencies. Moreover, if not calibrated correctly, downsampling can cause loss of detail in the signal. The results are in agreement with [45] where it is also shown that the technique is more efficient the lower the noise. Overall, the profiles obtained demonstrate that dual domain deconvolution represents a good compromise between computational stability and signal reconstruction accuracy.

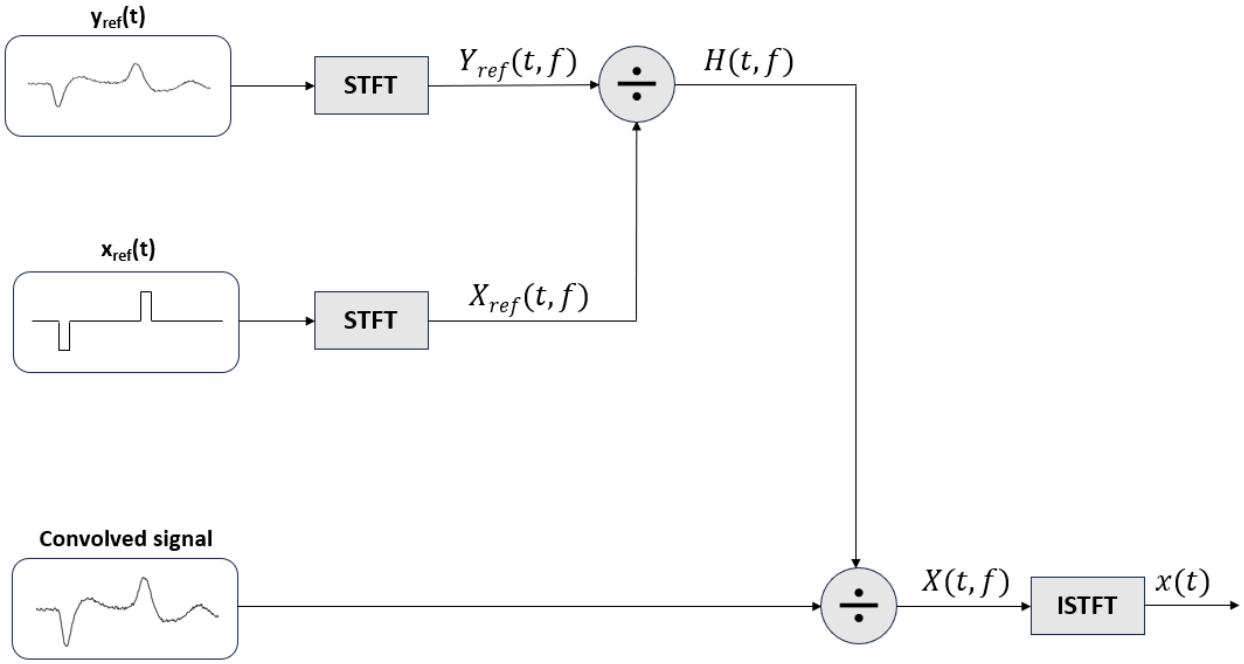

Fig. 23. Block diagram for the implementation of STFT based deconvolution.

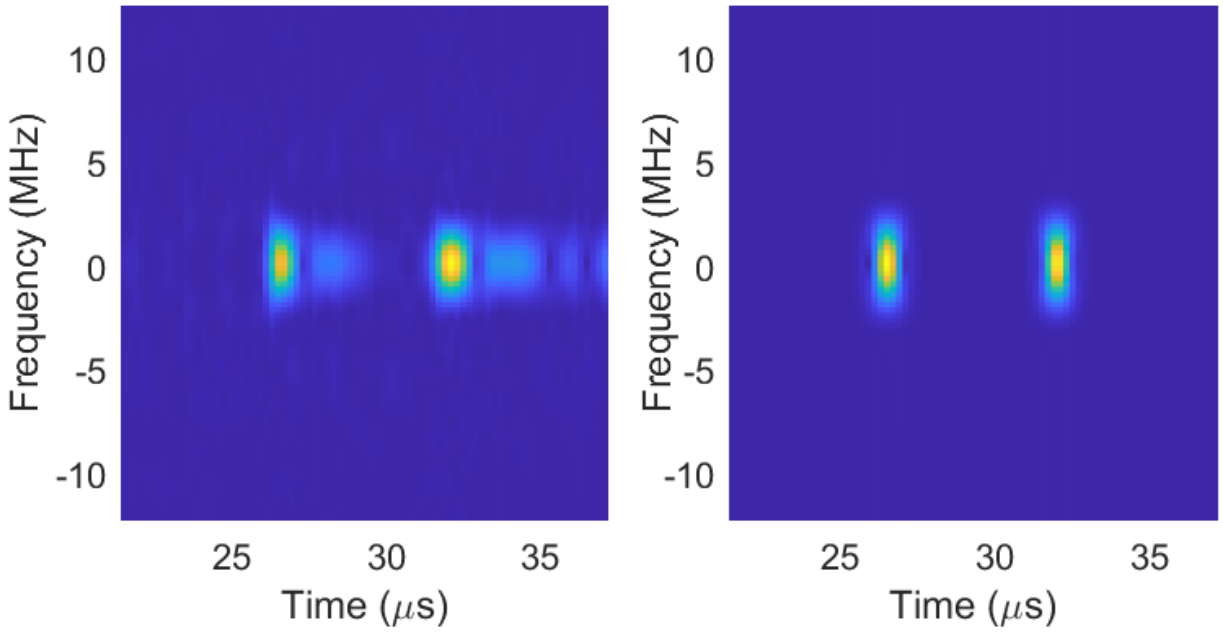

Fig. 24. Spectrogram of the measured reference signal, $y_{ref}(t)$ (left) and the deconvolved reference profile, $x_{ref}(t)$ (right).

G. Short Time Fourier Transform Based Deconvolution

Zhao et al. propose a Short Time Fourier Transform (STFT) based deconvolution technique to enhance the recovery of space charge signals in HVDC power cables [48]. This approach leverages the STFT's ability to provide a time-frequency representation of signals, transforming the deconvolution operation in the time domain into a localized division in the time-frequency domain. The technique is an extension of the classical Fourier Transform, which only provides a global representation of the frequencies present in a signal, without information on their temporal evolution. It enables the analysis of non-stationary signals, i.e. signals whose frequency content changes over time. The principle of the STFT is to divide the signal into short time segments, each of which is analyzed separately with the Fourier Transform. This is done using a moving window that selects a portion of the signal for each time instant. Mathematically, the STFT of a signal, $x(t)$, is defined as:

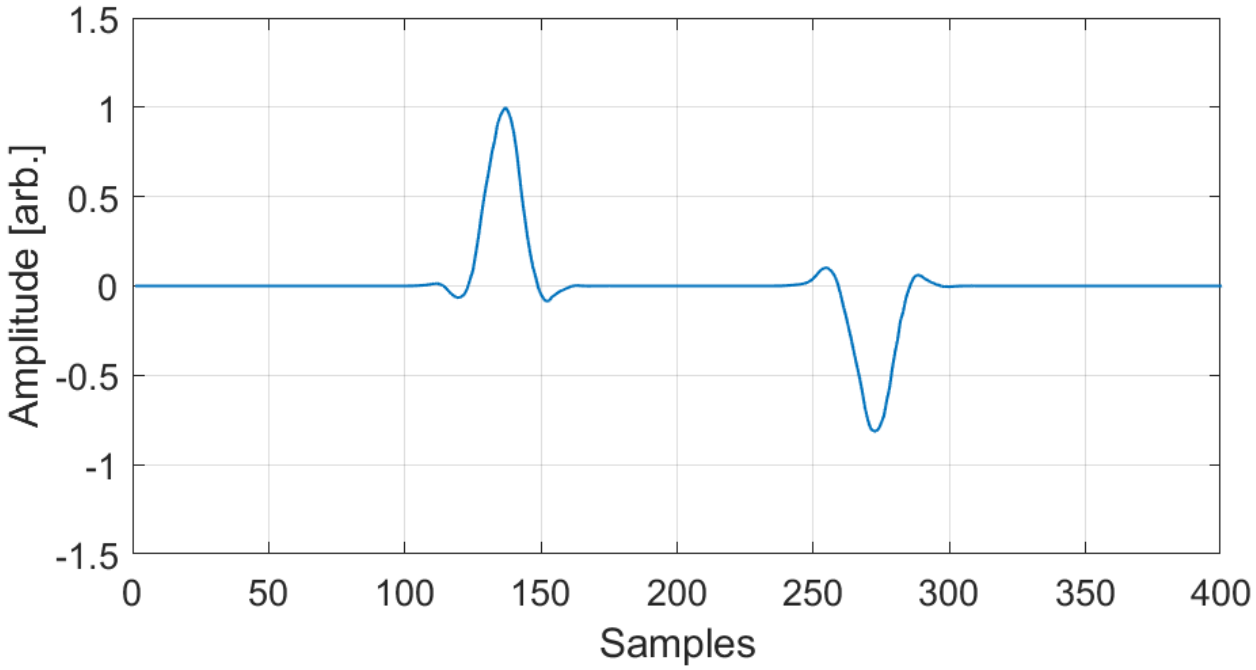

Fig. 25. Deconvolved model cable profile with STFT-Based method.

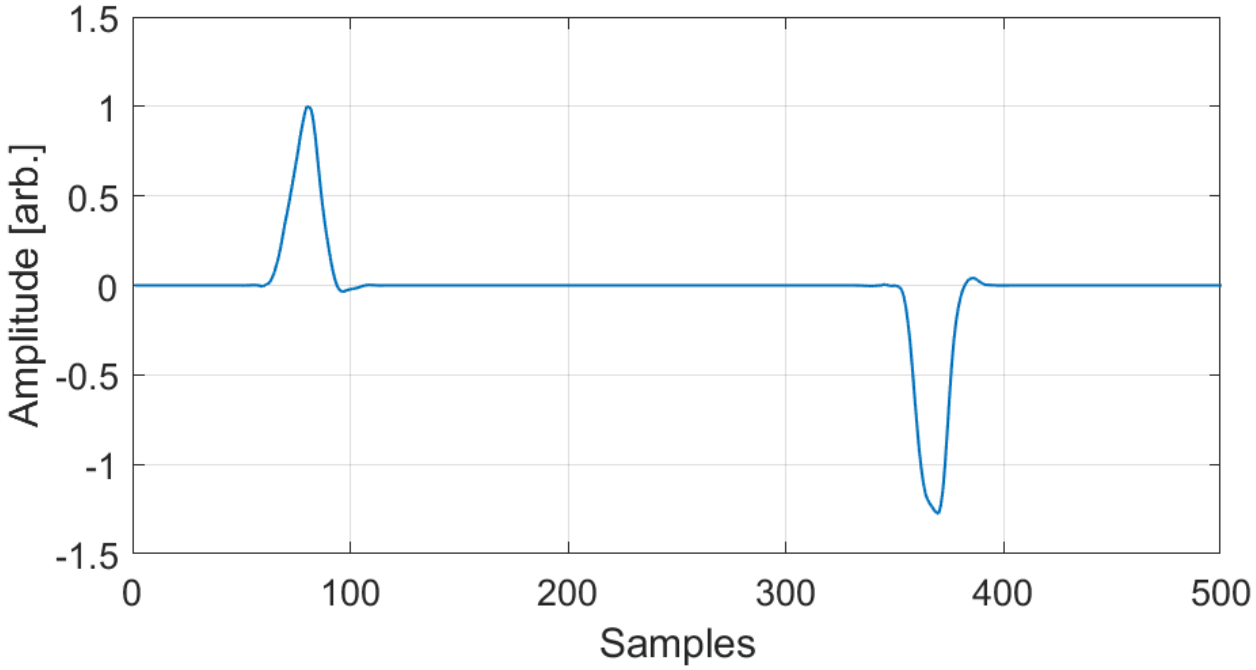

Fig. 26. Deconvolved full-size cable profile with STFT-Based method.

$$X(t,f) = \int_{-\infty}^{+\infty} x(t)w(t-\tau)e^{-j2\pi ft}dt \tag{19}$$

where $w(t-\tau)$ is a window function centered at instant τ. Since in [48] is not specified, a Hamming window has been used for this analysis. While fixed-shape windows such as Hamming, Hann, or Blackman provide comparable performance in most cases, the choice of window can influence the balance between temporal and spectral resolution. In particular, adjustable windows, such as the Tukey or Gaussian window, may offer greater flexibility in controlling spectral artifatcs and adapting the analysis to different waveform characteristics [49]. These aspects are relevant when constructing the time-frequency representation of the signal, which is at the core of the method described below. The transformed signal is a complex function of two real variables: time and frequency. In [48] the approach used involves the calculation of the STFT of a reference signal, $y_{ref}(t)$, measured under low voltage level, and an input reference signal, $x_{ref}(t)$, representing the ideal deconvolved profile. By dividing these references element-wise in the time-frequency domain, the authors derive a time-frequency transfer matrix, $H(t,f)$, which is used to reconstruct the original signal, $X(t,f)$, by deconvolving the measured profile $Y(t,f)$. The procedure is similar to that given in Eq. 3 for Fourier deconvolution:

$$H(t,f) = \frac{Y_{ref}(t,f)}{X_{ref}(t,f)} \quad \rightarrow \quad X(t,f) = \frac{Y(t,f)}{H(t,f)} \tag{20}$$

Then, the deconvolved signal in the time domain is obtained by applying the Inverse Short Time Fourier Transform (ISTFT). Fig. 23 shows the diagram used for the implementation of STFT based deconvolution, while Fig. 24 shows the magnitude of the STFT, known as spectrogram, for the $y_{ref}(t)$ signal (left) and the $x_{ref}(t)$ signal (right), which in this analysis has been chosen as two unit pulses concentrated at the dielectric interfaces. Fig. 25 and Fig. 26 show the results obtained for the deconvolution of model and full-size cable profiles, respectively. In both cases, a well reconstructed profile is obtained, free of baseline distortion and with a high SNR. The results obtained confirm what was reported in [48] where the technique is compared with Fuorier deconvolution. However, in analogy to IBD, the solution is strongly influenced by the choice of the ideal reference $x_{ref}(t)$, which therefore does not guarantee its uniqueness. The quality of the STFT also depends on the choice of window function $w(t-\tau)$ and its width, which modifies the resolution in time or in frequency. In fact, according to uncertainty principle, it is not possible to achieve high accuracy in frequency and time simultaneously. A window that is too narrow leads to high temporal resolution but low frequency resolution. The generation of artifacts or distortions can therefore cause loss of quantitative information of the reconstructed signal, like the modification of the shape of the second peak in Fig. 26. While the use of STFT for deconvolution is not inherently novel, its application in this specific context provides valuable insights, enabling the recovery of clearer space charge profiles. This facilitates improved diagnostics and reliability assessments for HVDC insulation systems.

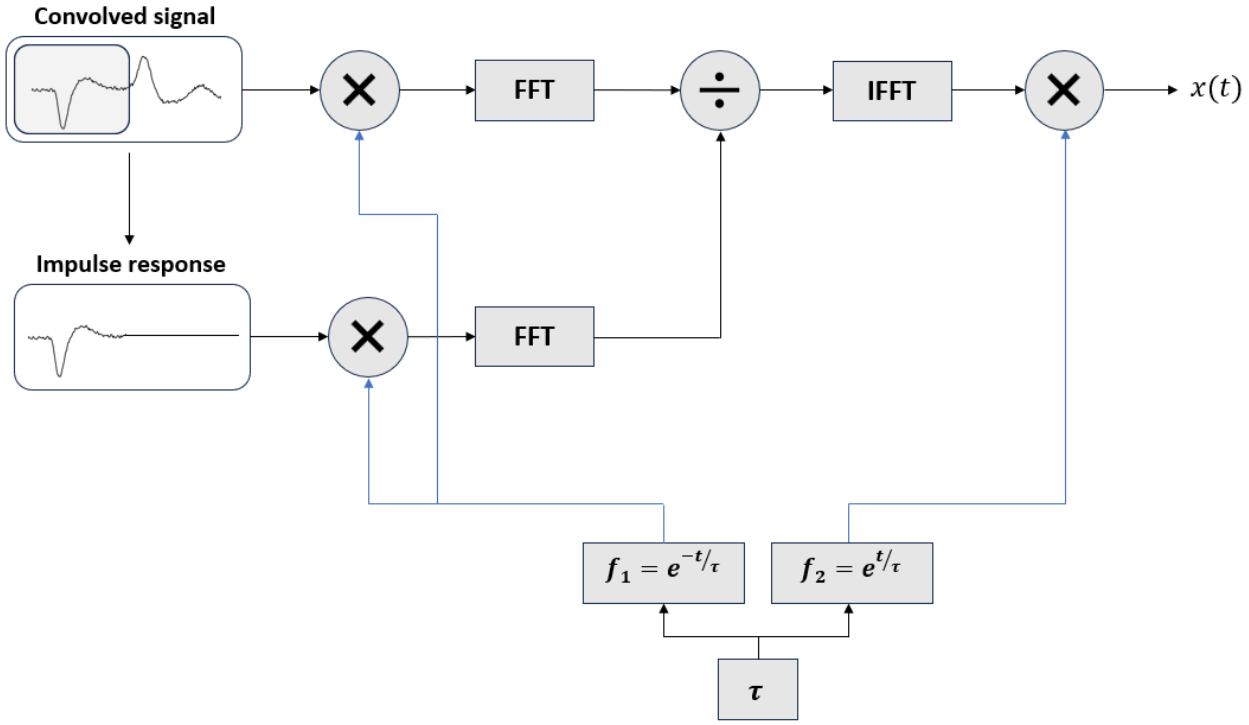

Fig. 27. Block diagram for the implementation of Laplace deconvolution.

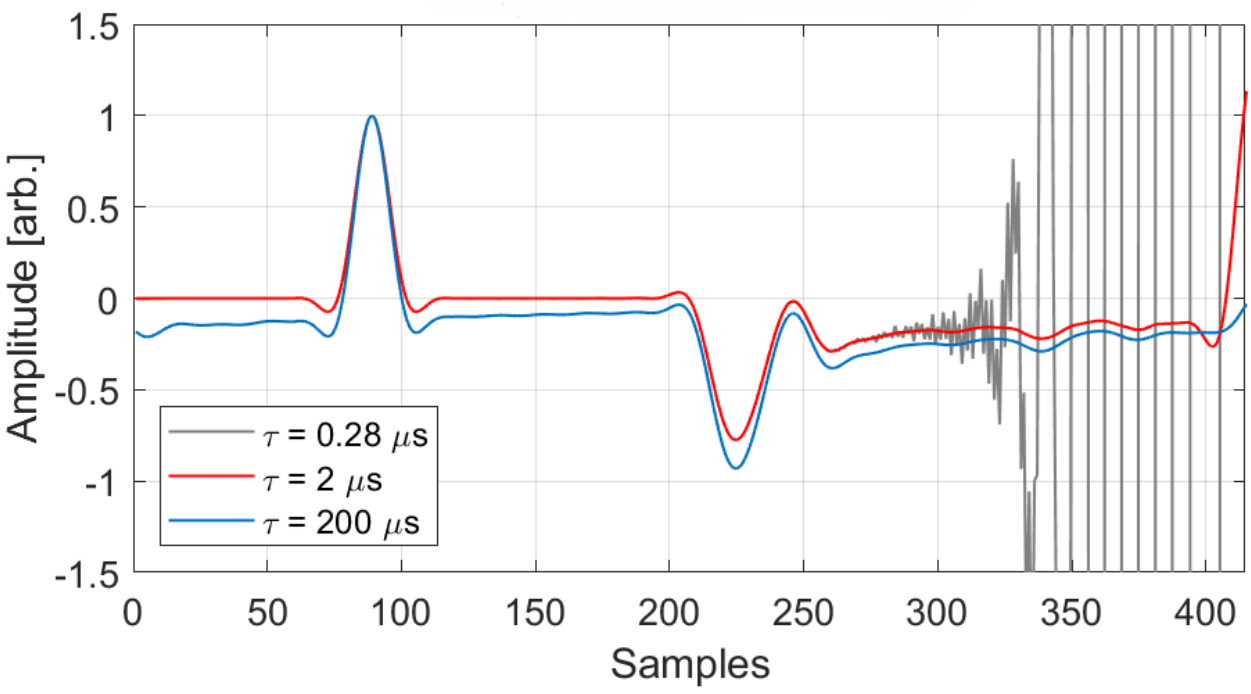

Fig. 28. Deconvolved model cable profile with Laplace deconvolution.

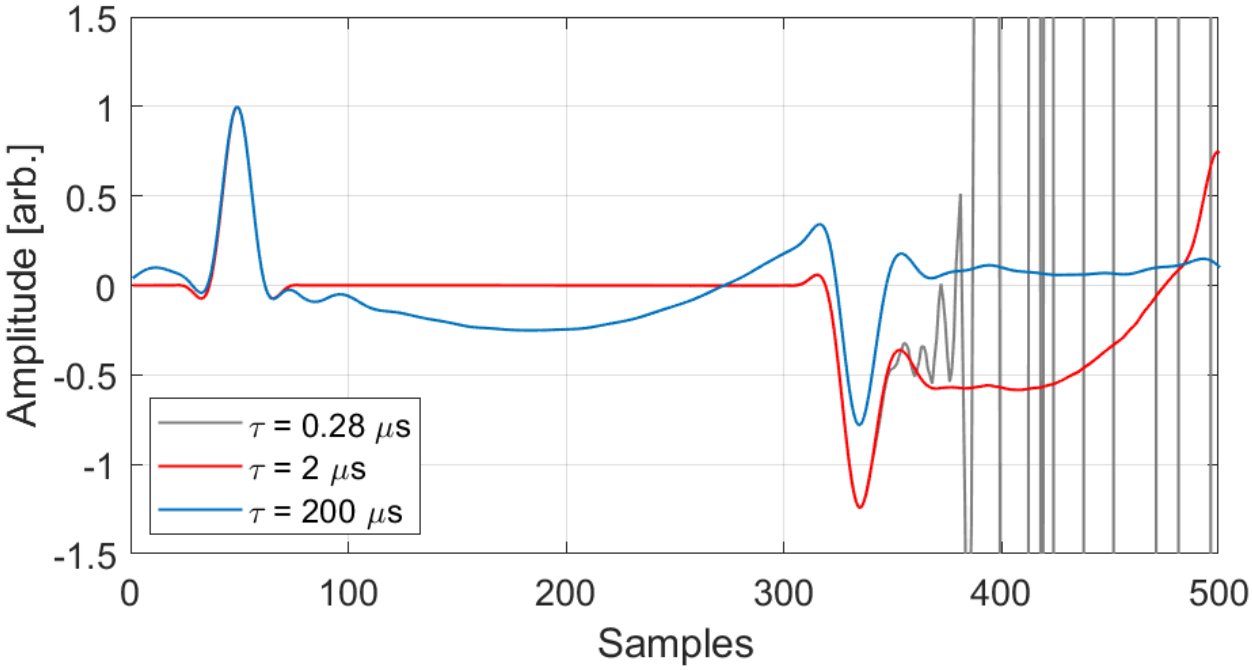

Fig. 29. Deconvolved full-size cable profile with Laplace deconvolution.

H. Laplace Deconvolution

In [50] the Laplace deconvolution technique has been suggested to improve the accuracy of reconstructing space charge profiles in HVDC insulation systems. Traditionally, PEA signals have been deconvolved in the frequency domain using the Fourier transform. However, when the measured signal exhibits long tails due to multiple reflections or not-optimal acoustic coupling, Fourier deconvolution can return signals that are not well processed. Long tails often do not converge to zero smoothly, introducing low-frequency components that distort the baseline. When truncation windows are applied to handle the tail, discontinuities may create spectral artifacts, further degrading the result. These challenges make Fourier deconvolution less effective for signals with slow-decaying tails, where Laplace deconvolution offers a more stable alternative by suppressing the tail's influence. In its general formulation, the Laplace transform has the following expression:

$$\mathcal{L}\{x(t)\} = \int_{-\infty}^{\infty} x(t) e^{-\left(\frac{1}{\tau}+j\omega\right)t} dt \tag{21}$$

where τ and ω are real variables. By decomposing the exponential term and introducing the following quantity:

$$\tilde{x}(t) = x(t) e^{-\frac{t}{\tau}} \tag{22}$$

it is possible to use τ to reduce the influence of the tails on the signal to be deconvolved. In this case, in fact, the Fourier transform of the signal $\tilde{x}(t)$ coincides with the Laplace transform of $x(t)$ for a fixed value of τ:

$$\mathcal{F}\{\tilde{x}(t)\} = \int_{-\infty}^{\infty} \tilde{x}(t) e^{-j\omega t} dt \tag{23}$$

Laplace deconvolution leverages the concept of the Laplace transform, which incorporates a time constant parameter, τ, to modulate the signal. This parameter allows the technique to emphasize the initial part of the signal while suppressing the tail, improving baseline stability and reducing artifacts. Although the numerical implementation employs the Fourier transform, particularly through the FFT for computational efficiency, the conceptual framework is derived from the Laplace domain, which is better suited for handling signals with slow decaying tails or distortions. The term "Laplace deconvolution" is used because the method is rooted in the principles of the Laplace transform, which generalizes the Fourier transform. By tuning τ, the exponential weighting modifies the frequency spectrum of $x(t)$ in a manner that mimics the behavior of a Laplace transform. When τ is large, the Laplace transform converges to the Fourier transform, losing its specific advantages. Conversely, smaller τ values suppress the influence of the signal tail, minimizing distortions caused by unwanted low-frequency components. This flexibility in adjusting τ allows Laplace deconvolution to offer a more robust and stable alternative for processing PEA signals, particularly in scenarios where traditional Fourier deconvolution struggles with baseline distortion and noise amplification. In Fig. 27 a block diagram summarizing the procedure for applying Laplace deconvolution is reported [10]. Once the deconvolution in the frequency domain is realised, the signal in the time domain is derived by means of an inverse transform, also considering the reconstruction of the tails by multiplication by an increasing exponential. Fig. 28 and Fig. 29 illustrate the results of Laplace deconvolution applied to the PEA signal for mini and full-size cable for three different values of the time constant τ. In both cases the parameter significantly influences the shape of the reconstructed signal by modulating the exponential weighting factor. For smaller values of τ (0.28 μs, gray line), the exponential weighting effectively suppresses the influence of the signal's tail, but this comes at the cost of increased noise amplification, as evidenced by the oscillatory artifacts. For larger values (200 μs, blue line), the weighting has minimal effect on the tail, preserving a smoother baseline but reducing the ability to suppress low-frequency distortions introduced by the tail. An intermediate value of 2 μs (red line), strikes a balance, providing better noise suppression and baseline stability,

though it may slightly under-represent rapid signal changes. This demonstrates how the tuning can optimize Laplace deconvolution for specific signal characteristics. Once again, the results are in agreement with what was reported in [10].

IV. Discussion

The comparative analysis of deconvolution techniques for PEA signal processing highlights the trade-offs between computational complexity, noise suppression, and reconstruction accuracy. Each method presents unique advantages and limitations that influence its applicability to different scenarios. For frequency domain approaches Fourier and Wiener deconvolution offer computational efficiency and straightforward implementation. However, these methods amplify high-frequency noise and suffer from baseline distortions, making them less reliable when the system transfer function is not well characterized. Wiener deconvolution provides some noise suppression by incorporating statistical noise estimation, but its effectiveness depends on the accuracy of the noise model unless it is decided to introduce a control parameter. Its iterative application by means of IBD bypasses the problem of baseline distortion and exact knowledge of the transfer function but requires an initial condition that does not guarantee the uniqueness of the solution. Time domain approaches such as direct time-domain deconvolution and sparse deconvolution provide improved baseline stability and reduced spurious low-frequency components. Sparse deconvolution, in particular, enhances resolution and is highly effective in detecting tiny localized charge accumulations. However, time-domain approaches require solving ill-conditioned inverse problems, making them computationally demanding and dependent on careful parameter tuning. Hybrid techniques achieve a balance between computational efficiency and reconstruction accuracy. The STFT-based method improves signal reconstruction by adapting to time-frequency signal analysis, while Laplace deconvolution mitigates long-tail distortions and enhances baseline stability. These methods offer promising alternatives for real-world HVDC cable diagnostics but require careful calibration of parameters such as transition frequencies, windowing functions, or time constants. The comparison findings are summarized in Table II. Interestingly, this analysis did not reveal substantial differences in the performance of these deconvolution techniques when applied to model cables versus full-size cables, suggesting that the primary challenges in PEA signal deconvolution are often intrinsic to the signal characteristics and algorithm limitations rather than being heavily dependent on the cable's scale. The problem of deconvolution manifests itself in many fields, especially in image processing, where more sophisticated algorithm applications

including machine learning and deep learning are already in place [51]. Further research should explore these new frontier of deconvolution techniques, i.e. for transfer function estimation, leveraging data-driven approaches to optimize signal reconstruction. Additionally, real-time implementation of advanced deconvolution methods could enhance on-site HVDC cable diagnostics, improving the predictive maintenance of insulation systems.

V. Conclusion

The study of space charge in HVDC insulation systems can be useful to evaluate and ensure the reliability of power cables. In this context, deconvolution techniques have been widely used to reconstruct space charge profile from raw signals acquired with the PEA method, reducing distortions introduced by the measurement system. This work presents a comprehensive review of the deconvolution approaches that have been found in the literature, analyzing their theoretical principles, advantages, and limitations. In addition to the theoretical review, the techniques have been implemented and compared through tests on PEA signals acquired from real measurements. The results obtained were also compared with those reported in the cited papers, which verified the consistency and reliability of the applied methodologies. The comparative analysis highlighted that the choice of the most appropriate deconvolution technique depends on several factors, including computational limitations, noise levels, and specific application requirements. While frequency domain methods offer greater computational efficiency, time domain methods, and hybrid approaches ensure higher accuracy also for complex measurement conditions. Future developments should focus on enhancing deconvolution algorithms for real-time applications, integrating adaptive techniques and machine learning-based approaches to enhance the robustness and automation of signal processing. The refinement of these methodologies represents a significant step forward in the advancement of HVDC insulation diagnostics, contributing to more efficient monitoring and maintenance systems for the electrical grids of the future.

References

[1] G. Arcia-Garibaldi, P. Cruz-Romero, and A. Gómez-Expósito, "Future power transmission: Visions, technologies and challenges," *Renewable and Sustainable Energy Reviews*, vol. 94, pp. 285–301, 2018.

[2] A. Alassi, S. Bañales, O. Ellabban, G. Adam, and C. MacIver, "Hvdc transmission: Technology review, market trends and future outlook," *Renewable and Sustainable Energy Reviews*, vol. 112, pp. 530–554, 2019.

[3] E. Pierri, O. Binder, N. G. Hemdan, and M. Kurrat, "Challenges and opportunities for a european hvdc grid," *Renewable and Sustainable Energy Reviews*, vol. 70, pp. 427–456, 2017.

Fourier	[20]–[29]	Inverse convolution in the Fourier domain	Computationally efficient, easy to implement with FFT	Noise amplification, baseline distortion	Low and high frequencies	Signals with high SNR
Wiener	[30]–[33]	Inverse convolution in the Fourier domain with integrated filter	Easy to implement, integrated denoising	Requires noise model, baseline distortion	Low frequencies	Signals with low SNR
IBD	[34]–[36]	Iterative algorithm with signal and transfer function estimation	No prior knowledge of transfer function needed	Non-unique solution	High frequencies	Cell with unknown or complex transfer function
Time Domain						
Time Domain	[23], [37]–[39]	Signal estimation with regression method and regularization technique	Preserves low-frequency components, reduces baseline distortions	High computational cost, requires tuning parameter	High frequencies	Signals with strong convolution effects and with long decay tails
Sparse	[41]–[43]	Iterative algorithm for signal estimation with sparsity constraints	Enhances resolution, effective in noise suppression	Requires tuning parameter, potential loss of small signal details	\	Thin flat dielectric layers, microstructure analysis
Hybrid Domain						
Dual Domain	[44]–[47]	Combines time and frequency domain deconvolution	Reduces baseline distortions, enhances resolution, improves stability	High computational complexity, requires careful merging of the two domains	\	Signal with high SNR and strong convolution effects
		Inverse convolution	Reduces baseline distortions, preserves			Suitable for

[4] N. Othman, M. Piah, and Z. Adzis, "Charge distribution measurement of solid insulator materials: A review and new approach," *Renewable and Sustainable Energy Reviews*, vol. 70, pp. 413–426, 2017.

[5] S. Govindarajan, A. Morales, J. A. Ardila-Rey, and N. Purushothaman, "A review on partial discharge diagnosis in cables: Theory, techniques, and trends," *Measurement*, vol. 216, p. 112882, 2023.

[6] L. A. Dissado and J. C. Fothergill, *Electrical degradation and breakdown in polymers*, vol. 9. Iet, 1992.

[7] G. Mazzanti and M. Marzinotto, "Extruded cables for high-voltage direct-current transmission: advances in research and development," 2013.

[8] B. Du, *Polymer Insulation Applied for HVDC Transmission*. Springer Nature, 2020.

[9] P. Morshuis and M. Jeroense, "Space charge measurements on impregnated paper: a review of the pea method and a discussion of results," *IEEE Electrical Insulation Magazine*, vol. 13, no. 3, pp. 26–35, 1997.

[10] N. Hozumi, "Space charge measurement techniques for practical insulation systems," in *2023 IEEE 4th International Conference on Electrical Materials and Power Equipment (ICEMPE)*, pp. 1–8, 2023.

[11] A. Imburgia, R. Miceli, E. R. Sanseverino, P. Romano, and F. Viola, "Review of space charge measurement systems: acoustic, thermal and optical methods," *IEEE Transactions on Dielectrics and Electrical Insulation*, vol. 23, no. 5, pp. 3126–3142, 2016.

[12] G. Rizzo, P. Romano, A. Imburgia, and G. Ala, "Review of the pea method for space charge measurements on hvdc cables and mini-cables," *Energies*, vol. 12, no. 18, 2019.

[13] A. Imburgia, P. Romano, G. Chen, G. Rizzo, E. Riva Sanseverino, F. Viola, and G. Ala, "The industrial applicability of pea space charge measurements, for performance optimization of hvdc power cables," *Energies*, vol. 12, no. 21, p. 4186, 2019.

[14] M. Fu, G. Chen, A. Davies, and J. Head, "Space charge measurements in cables using the pea method:-signal data processing considerations," in *ICSD'01. Proceedings of the 20001 IEEE 7th International Conference on Solid Dielectrics (Cat. No.01CH37117)*, pp. 219–222, 2001.

[15] M. Fu and G. Chen, "Space charge measurement in polymer insulated power cables using flat ground electrode pea system," vol. 150, pp. 89–96, IET, 2003.

[16] A. Di Fatta, P. Romano, G. Rizzo, G. Ala, and A. Imburgia, "The interaction between electric field and partial discharges simultaneously detected in a hvdc cable under operating conditions," *IEEE Access*, vol. 12, pp. 140171–140184, 2024.

[17] R. Bracewell and P. B. Kahn, "The fourier transform and its applications," *American Journal of Physics*, vol. 34, no. 8, pp. 712–712, 1966.

[18] P. Romano, A. Imburgia, G. Rizzo, A. Di Fatta, G. Akbar, F. Viola, G. Berardi, M. Albertini, S. F. Bononi, and G. Ala, "Development of a new pea cell for model cables," in *2023 IEEE Conference on Electrical Insulation and Dielectric Phenomena (CEIDP)*, pp. 1–4, 2023.

[19] A. Imburgia, P. Romano, G. Rizzo, A. Di Fatta, G. Akbar, F. Viola, G. Berardi, M. Albertini, S. F. Bononi, and G. Ala, "Simulation of a new developed pea cell for flat specimens and full-size cables," in *2023 IEEE Conference on Electrical Insulation and Dielectric Phenomena (CEIDP)*, pp. 1–4, 2023.

[20] T. Maeno, T. Futami, H. Kushibe, T. Takada, and C. Cooke, "Measurement of spatial charge distribution in thick dielectrics using the pulsed electroacoustic method," *IEEE Transactions on Electrical Insulation*, vol. 23, no. 3, pp. 433–439, 1988.

[21] H.-C. Jung, H.-G. Kim, T.-I. Choi, and S. Hwangbo, "Automatic measurement system of the space charge distribution by a two-step deconvolution," *Journal of Electrical Engineering & Technology*, vol. 14, pp. 2049–2055, 2019.

[22] T. Takada, Y. Tanaka, N. Adachi, and X. Qin, "Comparison between the pea method and the pwp method for space charge measurement in solid dielectrics," *IEEE Transactions on Dielectrics and Electrical Insulation*, vol. 5, no. 6, pp. 944–951, 1998.

[23] B. Vissouvanadin, T. T. N. Vu, L. Berquez, S. L. Roy, G. Teyssèdre, and C. Laurent, "Deconvolution techniques for space charge recovery using pulsed electroacoustic method in coaxial geometry," *IEEE Transactions on Dielectrics and Electrical Insulation*, vol. 21, no. 2, pp. 821–828, 2014.

[24] T. T. N. Vu, G. Teyssedre, and L. Berquez, "Space charge measurement by PEA electroacoustic method : impact of acoustic properties of materials on the response for different geometries," *International Journal on Electrical Engineering and Informatics*, no. 2, 2018.

[25] W. Min, J. Kang, H. Kim, J. Park, and S. Hwangbo, "A study on the correction processing for the signal of the space charge distribution in polymer insulating materials measured by pea method," *The Transactions of The Korean Institute of Electrical Engineers*, vol. 67, no. 7, pp. 860–864, 2018.

[26] G. Chen, Y. L. Chong, and M. Fu, "Calibration of the pulsed electroacoustic technique in the presence of trapped charge," *Measurement Science and Technology*, vol. 17, p. 1974, jun 2006.

[27] D. van der Born, "Investigation of space charge injection, conduction and trapping mechanisms in polymeric hvdc mini-cables," *TU Delft, Delft University of Technology*, 2011.

[28] M. Fu, *Space charge measurement in polymer insulated power cables using the PEA method*. PhD thesis, University of Southampton, 2002.

[29] Y. Zhan, *Space charge modelling and measurement in HVDC extruded cable insulation*. PhD thesis, University of Southampton, 2020.

[30] M. J. P. Jeroense, "Charges and discharges in hvdc cables-in particular in mass-impregnated hvdc cables," 1997.

[31] K. Hencken and A. Abbasi, "Analysis of the deconvolution and reconstruction of pea signals for hv insulation materials," in *2016 IEEE International Conference on Dielectrics (ICD)*, vol. 2, pp. 926–929, 2016.

[32] L. H. Pearson, J. R. Dennison, E. W. Griffiths, and A. C. Pearson, "Pea system modeling and signal processing for measurement of volume charge distributions in thin dielectric films," *IEEE Transactions on Plasma Science*, vol. 45, no. 8, pp. 1955–1964, 2017.

[33] A. Gupta and C. Chakradhar Reddy, "Analytical insights into parameter estimation for wiener deconvolution," *IEEE Transactions on Instrumentation and Measurement*, vol. 66, no. 10, pp. 2566–2575, 2017.

[34] D. Kundur and D. Hatzinakos, "Blind image deconvolution," *IEEE Signal Processing Magazine*, vol. 13, no. 3, pp. 43–64, 1996.

[35] D. Kundur and D. Hatzinakos, "Blind image deconvolution revisited," *IEEE Signal Processing Magazine*, vol. 13, no. 6, pp. 61–63, 1996.

[36] A. Gupta and C. C. Reddy, "A comparative study of de-convolution methods for charge signal estimation in pea system," in *2022 IEEE 7th International Conference on Recent Advances and Innovations in Engineering (ICRAIE)*, vol. 7, pp. 494–499, 2022.

[37] N. Fuse, S. Morita, S. Miyazaki, T. Takahashi, and N. Hozumi, "Estimation accuracy of the electric field in cable insulation based on space charge measurement," *Energies*, vol. 15, no. 13, p. 4920, 2022.

[38] N. Fuse, S. Morita, S. Miyazaki, T. Takahashi, and N. Hozumi, "Estimation accuracy of electric field in cable-insulating wall based on space charge measurement," in *2022 IEEE Conference on Electrical Insulation and Dielectric Phenomena (CEIDP)*, pp. 32–35, 2022.

[39] X. Li, Y. An, T. Kawashima, Y. Murakami, and N. Hozumi, "Transfer matrix for space-charge analysis of insulating systems with complex geometries," in *2023IEEE 4th InternationalConferenceonElectricalMaterialsandPowerEquipment (ICEMPE)*, pp. 1–4, 2023.

[40] P. C. Hansen, "Analysis of discrete ill-posed problems by means of the l-curve," *SIAM review*, vol. 34, no. 4, pp. 561–580, 1992.

[41] A. Gupta and C. C. Reddy, "Sparse de-convolution of space charge signal in pea method," in *2013 IEEE International Conference on Signal Processing, Computing and Control (ISPCC)*, pp. 1–4, 2013.

[42] I. Selesnick, "Sparse deconvolution (an mm algorithm)," *Connexions*, pp. http–cnx, 2012.

[43] A. Gholami and M. D. Sacchi, "A fast and automatic sparse deconvolution in the presence of outliers," *IEEE Transactions on Geoscience and Remote Sensing*, vol. 50, no. 10, pp. 4105–4116, 2012.

[44] E. B. Prastika, A. Imori, T. Kawashima, Y. Murakami, N. Hozumi, S. Yoshida, R. Nagaoka, and K. Kobayashi, "Acoustic impedance interpretation of cross-sectional human skin by using time and frequency domain deconvolution," *Japanese Journal of Applied Physics*, vol. 59, p. SKKB06, apr 2020.

[45] N. Hozumi, E. B. Prastika, S. Zahra, T. Kawashima, and Y. Murakami, "Dual-domain deconvolution process applied to time-resolved quantitative dielectric measurement," in *2020 IEEE 3rd International Conference on Dielectrics (ICD)*, pp. 347–350, 2020.

[46] E. Bagus Prastika and N. Hozumi, "The application of signal processing using dual domain deconvolution for new space charge measurement method in hvdc full-size cables," 01 2021.

[47] S. Zahra, S. Morita, M. Utagawa, T. Kawashima, Y. Murakami, N. Hozumi, P. Morshuis, Y.-I. Cho, and Y.-H. Kim, "Space charge measurement equipment for full-scale hvdc cables using electrically insulating polymeric acoustic coupler," *IEEE Transactions on Dielectrics and Electrical Insulation*, vol. 29, no. 3, pp. 1053–1061, 2022.

[48] J. Zhao, Y. Ge, J. Chen, S. Wang, and K. Wu, "An improved space charge measurement approach for power cables," *IEEE Transactions on Instrumentation and Measurement*, vol. 73, pp. 1–7, 2024.

[49] K. M. Prabhu, *Window functions and their applications in signal processing*. Taylor & Francis, 2014.

[50] A. Yeongguk, X. Li, T. Kawashima, Y. Murakami, and N. Hozumi, "Signal processing for space charge measurement using laplace deconvolution," in *2022 9th International Conference on Condition Monitoring and Diagnosis (CMD)*, pp. 811–814, 2022.

[51] M. Makarkin and D. Bratashov, "State-of-the-art approaches for image deconvolution problems, including modern deep learning architectures," *Micromachines*, vol. 12, no. 12, p. 1558, 2021.

Alessio Di Fatta received his Master's degree in electrical engineering from the University of Palermo, Italy, in 2022. Since 2022, he has been working as a Ph.D. with the Department of Engineering, University of Palermo. His research interest include HVDC systems, partial discharge measurement and pattern recognition algorithms, space charge accumulation and insulating systems diagnosis.

Giuseppe Rizzo was born in 1984. He obtained the Master's degree in Nuclear Engineering at the University of Palermo in 2008. From 2009 to 2018, he worked as a researcher and designer of Small Wind Turbine Generators (SWTG) at Jonica Impianti. In 2021, he obtained the Ph.D. at the University of Palermo defending a thesis focused on the role of space charge phenomena in HVDC applications. Since 2021, he has been employed in EOSS (Prysmian Group) as R&D software engineer and his activity is focused on the development of Real Time Thermal Rating algorithms.

Pietro Romano (SM '17) received his MSc and PhD degrees in electrical engineering from the University of Palermo, Italy, in 1993 and 1998, respectively. He is full professor with the Department of Engineering at the University of Palermo and teaches basic electrical engineering, electrotechnics and insulation systems diagnostics. His research activity is mainly in the fields of insulating systems diagnosis, partial discharge, and space charge measurements, HV systems, HVDC cable systems, multifactor stress effects and electric field simulations. He is the head of the L.E.PR.E. HV Laboratory, Palermo University. He is member of Italian AG of the European SET Plan WG HVDC, IEEE DEIS Meetings Committee, IEEE DEIS CEIDP Board, IEEE DEIS ICD Committee and CIGRÉ AG D1.03 "Solid materials".

Guido Ala is currently a Full Professor in electrical engineering at the "Dipartimento di Ingegneria", University of Palermo, Italy. Since 2012, he has been the Director of the Laboratory for Modeling and Electromagnetic Simulation (MOSEM-Lab). His main research interests ar in the fields of computational electromagnetics (including MoM, FDTD, application of wavelets, mesh-free innovative numerical approach), electromagnetic transient analysis, lightning, electromagnetic compatibility, optimized design of EMI filters and power electronics converters, partial discharge detection, biomedical engineering (including magnetoencephalography and electroencephalography innovative numerical modeling, and electromagnetic fields effect on humans), electrical systems design for fusion engineering, innovative solutions for sustainable mobility (including photovoltaic applications) in the smart cities context, electrical analogies in material's viscoelasticity behavior.

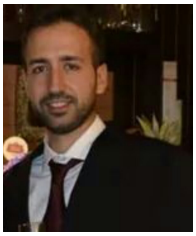

Antonino Imburgia received his M.Sc. degree in electrical engineering from the University of Palermo, Italy, in 2014. Since 2015, he has been working as a Ph.D. and as a researcher with the Department of Engineering, University of Palermo. His research interests include HVDC, distribution of space charge in solid dielectrics and its behavior, dielectrics and electrical insulating systems diagnosis, space charge and partial discharge measurements.